minerals

MDPI

Article

Deciphering Iberian Variscan Orogen Magmatism Using the Anisotropy of Magnetic Susceptibility from Granites

Helena Sant'Ovaia [1,2,*], Cláudia Cruz [1,2], Ana Gonçalves [2], Pedro Nogueira [3,4] and Fernando Noronha [1,2]

1 Departamento de Geociências, Ambiente e Ordenamento do Território, Faculdade de Ciências, Universidade do Porto, Rua do Campo Alegre, 687, 4169-007 Porto, Portugal; claudiacruz@fc.up.pt (C.C.); fmnoronh@fc.up.pt (F.N.)
2 Instituto de Ciências da Terra, Polo da Universidade do Porto, Rua do Campo Alegre, 687, 4169-007 Porto, Portugal; anagoncalves.geo@gmail.com
3 Departamento de Geociências, Universidade de Évora, Colégio Luís António Verney, Rua Romão Ramalho, 59, 7000-671 Évora, Portugal; pmn@uevora.pt
4 Instituto de Ciências da Terra, Polo da Universidade de Évora, Colégio Luís António Verney, Rua Romão Ramalho, 59, 7000-671 Évora, Portugal
* Correspondence: hsantov@fc.up.pt

Abstract: In this paper, we have synthesized the information derived from more than 20 papers and PhD theses on the anisotropy of the magnetic susceptibility (AMS) of 19 Variscan granite plutons, spanning the period between 320 Ma and 296 Ma. The AMS data are obtained from 876 sampling sites with more than 7080 AMS measurements and a re-interpretation is proposed. The studied granites exhibit a magnetic susceptibility (Km) ranging from 30 to 10,436 $\times$ 10^{-6} SI units. Most granites typically exhibit Km values below 1000 $\times$ 10^{-6} SI, indicative of paramagnetic behavior. Biotite serves as the main carrier of iron (Fe), emphasizing the reduced conditions prevalent during the formation of granite melts in the Variscan orogeny. The AMS fabrics of the studied granite plutons record the magma strain, expressing the chronologic evolution of the stress field during the orogeny. This chronologic approach highlights the magmatic events between around 330 and 315 Ma, occurring in an extensional regime, in which the Borralha pluton is an example of a suite that recorded this extensional AMS fabric. Plutons with ages between 315 and 305 Ma show AMS fabrics, pointing out their emplacement in a compressional tectonic regime related to the Variscan collision. The plutons, younger than 305 Ma, record AMS fabrics indicating that the tectonic setting for emplacement changes from a wrench regime to an extensional one at the end of the collision stage. This is evident as there is a chronological overlap between the granites that exhibit AMS fabrics indicating extension and the ones that have AMS fabrics indicating a wrench regime.

Keywords: granites; anisotropy of magnetic susceptibility; Variscan orogeny; magma strain

Citation: Sant'Ovaia, H.; Cruz, C.; Gonçalves, A.; Nogueira, P.; Noronha, F. Deciphering Iberian Variscan Orogen Magmatism Using the Anisotropy of Magnetic Susceptibility from Granites. *Minerals* **2024**, *14*, 309. https://doi.org/10.3390/min14030309

Academic Editor: Emilio L. Pueyo

Received: 20 December 2023
Revised: 1 March 2024
Accepted: 8 March 2024
Published: 15 March 2024

1. Introduction and Objectives

Anisotropy of magnetic susceptibility (AMS) studies on granites, conducted extensively in recent decades (e.g., [1–15]), provide new insights into the study of granitic bodies. A broad spectrum of applications exists, spanning from the utilization of magnetic susceptibility (Km) for mapping granite facies and correlating their susceptibility with geochemical features (e.g., [5]), to kinematic applications such as interpreting the emplacement mechanisms through the analysis of magnetic fabric (e.g., [12]). Furthermore, additional applications of the magnetic susceptibility of granites can be ascertained, as follows: as an indicator of metallogenic potential (e.g., [9,13]); as an indicator of hydrothermal alteration (e.g., [15]); or as a way of assessing magnetic mineralogy (e.g., [13]).

In the Iberian Peninsula, AMS studies have been extensively conducted on Variscan granites in both Portugal and Spain (e.g., [14–19]), but few data syntheses have been carried out so far (e.g., [10]).

The aim of this work is to summarize the AMS studies that have been carried out on Portuguese Variscan granites. These data were obtained over the last 20 years in the Anisotropy of Magnetic Susceptibility Laboratory of the Earth Sciences Institute of the University of Porto and were published as several articles and doctoral theses.

Nineteen Variscan granitic plutons located in Central and Northern Portugal, in the Central Iberian Zone (CIZ) and Galicia-Trás-os-Montes Zone (GTMZ) [20], with suitable AMS data available spanning the period between 320 Ma and 296 Ma were considered. The objectives of this work are as follows:

i. To understand the geologic significance of magnetic susceptibility data, considering the presence of biotite and/or muscovite, along with the magnetic behavior of these granites. This includes examining the paramagnetic and/or ferromagnetic (s.l.) mineralogy and establishing correlations with the redox conditions during magma genesis.
ii. To correlate magnetic anisotropy fabrics with macro- and microstructures observable in the granites and to interpret them in the context of the emplacement of these granites during the Variscan orogeny.
iii. To map the magnetic fabric of plutons with different ages within the Variscan orogen and to investigate the magma strain history recorded by these granites.
iv. Finally, to analyze the timing of the pluton's emplacement with relation to the Variscan orogeny, identifying the transitions between regional stress fields during the evolution of the orogen.

2. Anisotropy of Magnetic Susceptibility (AMS)

2.1. Theorethical Framework and Applications

When a mineral (or a rock) is exposed to a magnetic field, H, it acquires an induced magnetization, M. The induced magnetization and the magnetic field are directly related through the magnetic susceptibility, Km, which is expressed by the following mathematical expression:

$$\mathrm{M} = \mathrm{Km} \cdot \mathrm{H} \tag{1}$$

If the material is isotropic, the magnetic susceptibility is a scalar; if the material is anisotropic, the magnetic susceptibility is represented, as follows, by a symmetrical second order tensor of the form:

$$\mathrm{Mi} = \mathrm{Kij} \cdot \mathrm{Hj} (\mathrm{i}, \mathrm{j} = 1, 2, 3) \tag{2}$$

where Mi represents the magnetization in the i direction and Hj represents the magnetic field in the j direction. Given that M and H are expressed in amperes per meter (A/m), Km per volume is dimensionless (in the units of the International System, SI) (e.g., [4,21]). The magnetic susceptibility tensor is represented by a triaxial ellipsoid, whose three main orthogonal axes define the main magnetic directions (Figure 1). The Km values obtained along the main directions are the main susceptibilities, known as maximum (Kmax = K1), intermediate (Kint = K2), and minimum (Kmin = K3) susceptibilities [22].

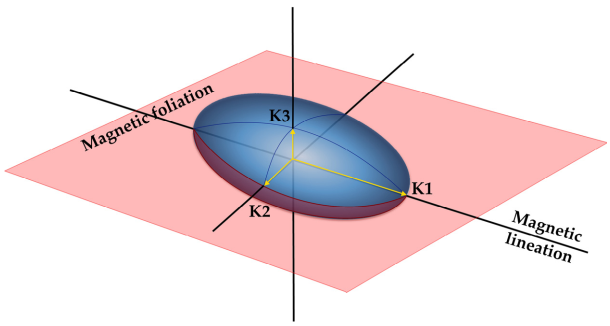

Figure 1. Schematic representation of the ASM triaxial ellipsoid. The magnetic foliation plane represents the plane perpendicular to K3 and the magnetic lineation axis represents the lineation parallel to K1. K1 = Kmax, K2 = Kint, and K3 = Kmin (adapted from Siegesmund [23]).

The Km of a rock results from the contribution of the magnetic susceptibilities of all the constituent minerals of the material under study, which can be (i) diamagnetic (e.g., quartz and feldspars), (ii) paramagnetic (e.g., biotite), (iii) antiferromagnetic (e.g., goethite), and (iv) ferromagnetic (s.l.), which includes ferromagnetic (s.s., e.g., iron), weak ferromagnetic (e.g., hematite), and ferrimagnetic (e.g., magnetite) [24,25].

In strongly magnetic rocks, with a Km higher than 5×10^{-3} SI, the effect of mafic silicates is negligible and the rock susceptibility is effectively controlled by magnetite only. In weakly magnetic rocks, with a Km lower than 5×10^{-4} SI, the content of ferromagnetic minerals is often so low that the susceptibility is effectively controlled by mafic silicates. In rocks with a Km between 5×10^{-4} and 5×10^{-3} SI, the AMS, in general, is controlled by both ferromagnetic and paramagnetic minerals [26].

The AMS is the magnetic anisotropy concerning the variation in the direction of the induced magnetization and, therefore, the dependence of the susceptibility in the direction along which it is being measured. At the scale of the mineral grain, the AMS is controlled by the crystallographic system and crystal orientation. AMS is also often influenced by the shape of the mineral grain, which overrides crystallographic control [24]. In general, the magmatic or tectonic fabrics in granites at the mesoscopic scale are planar and are marked by the preferential alignment of tabular or sheet-like minerals, such as micas and feldspars. This mineralogical fabric is often parallel to a planar magnetic fabric, the magnetic foliation, perpendicular to the Kmin direction of the AMS ellipsoid. Linear mineral fabrics are marked by the alignment of elongated or needle-like crystals, such as amphibole, and are parallel to the Kmax direction of the AMS ellipsoid, the magnetic lineation.

2.2. AMS Methods

To carry out AMS studies, it is necessary to collect oriented and regularly distributed samples of the granite under study. The methodology of AMS studies (e.g., [4]) is based on selecting a sampling site at each vertex of a kilometric quadrangular grid (which is not always possible due to factors such as the absence of outcrops, scarcity of in situ exposures, or excessive weathering). Sampling is carried out using a portable coring drill, whose sampler consists of a non-magnetic tube that ends in a diamond-bit crown. The sampler is cooled and lubricated using pressurized water using a manual external pump. At each sampling site, before gathering the ~25 mm diameter core samples, their orientation is determined using a compass and a non-magnetic orientator. The recorded values include the strike of the vertical plane containing the core axis and the plunge of the core axis. Oriented arrows, representing the trend and the direction of the core plunge, are marked on each core sample (Figure 2). From each site, several samples are collected to ensure that in the lab, after being cut to a height of ~22 mm, we are left with six to eight samples to ensure statistical reliability (e.g., [4]). The exact dimensions (the diameter and height) of each sample are then used to calculate its volume, which is used to determine the magnetic susceptibility (per unit of volume). Finally, magnetic susceptibility measurements are carried out using a Kappabridge susceptibility balance from Agico (Brno, Czech Republic). The data presented here were obtained in the KLY-4S model, which measures the AMS of a spinning specimen fixed in the rotator, with the software SUFAR that combines the measurements in three perpendicular planes plus one bulk value to create a complete magnetic susceptibility tensor (www.agico.com, accessed on 15 December 2023).

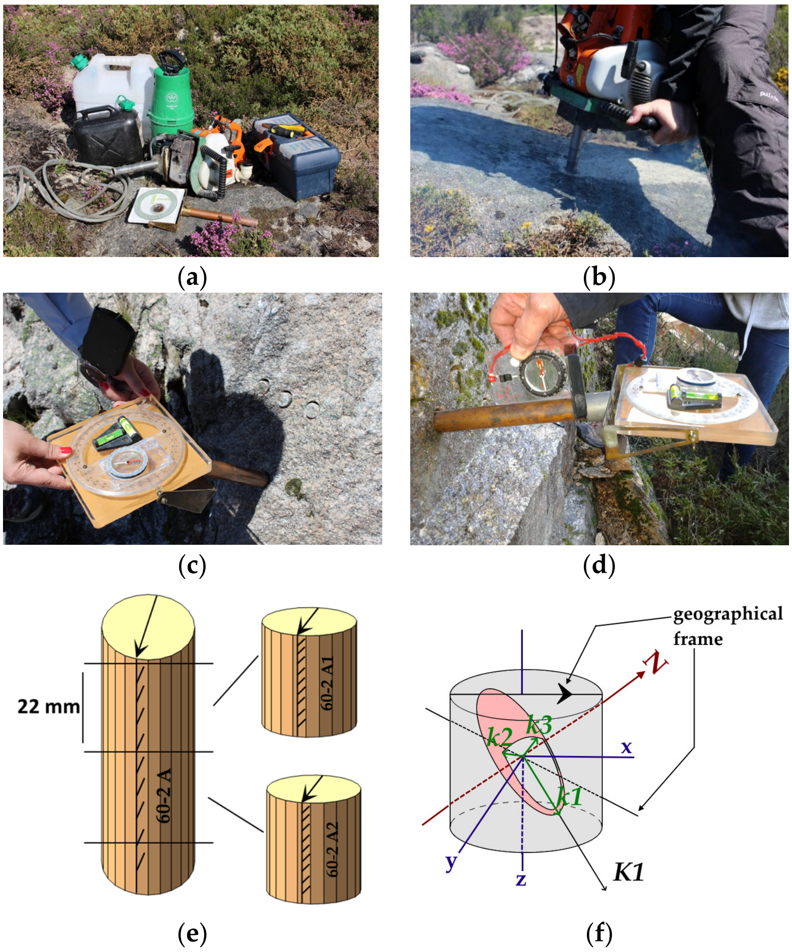

Figure 2. Oriented samples for the AMS procedure. (**a**) AMS sampling equipment. (**b**) Drilling with portable equipment. (**c**,**d**) Measuring the orientation of the core in situ (trend and plunge). (**e**) Oriented sample and sub-samples. (**f**) Using the trend and plunge of the core axis, the AMS ellipsoid is calculated back to the geographical frame.

2.3. AMS Parameters

Measurements performed using the Kappabridge allow us to define the intensity and direction of the three principal axes, K1 ≥ K2 ≥ K3, of the AMS ellipsoid of each sample. Means of the tensor axes corresponding to the n samples measured at a site are K1 ≥ K2 ≥ K3 and are obtained using the ANISOFT 4.2 program package (www.agico.com, accessed on 15 December 2023).

The mean susceptibility value, Km, is calculated using the following equation:

$$\mathrm{Km} = \frac{\mathrm{K1} + \mathrm{K2} + \mathrm{K3}}{3} \quad (3)$$

The degree of magnetic anisotropy (P%) is calculated using the following equation:

$$\mathrm{P}(\%) = \left(\frac{\mathrm{K1}}{\mathrm{K3}} - 1\right) \times 100 \quad (4)$$

The mean direction and confidence angles of the axes K1 and K3, in terms of azimuth and plunge, were calculated using directional statistics based on the Bingham distribution. For each site, magnetic lineation, parallel to the direction of K1, and magnetic foliation, which is represented by the plane perpendicular to K3, are defined.

3. Iberian Variscan Belt

The pre-Mesozoic terrains in SW Europe have ages ranging from the Proterozoic to the Upper Carboniferous. These terrains, deformed and metamorphosed, are often intruded by Variscan granites characterized by significant geochemical and textural variability. Together, these geological features characterize the Variscan belt that extends from the south of Iberia to the northeast of Bohemia [27–30].

The Variscan belt was shaped by the convergence and collision between the supercontinents Laurussia and Gondwana, after the closure of the Rheic Ocean.

The westernmost part of this belt corresponds to the Iberian Variscan Belt (IBV), which is subdivided into six palaeogeographic zones as follows, each having specific tectonic, geologic, metamorphic, and stratigraphic characteristics [20,31,32]: (i) the Cantabrian Zone, (ii) the West Asturian-Leonese Zone, (iii) the Galicia-Trás-os-Montes Zone (GTMZ), (iv) the Central Iberian Zone (CIZ), (v) the Ossa-Morena Zone (OMZ), and (vi) the South Portuguese Zone.

Currently, two distinct models are in discussion to explain the tectonic evolution of the IVB and its corresponding magmatism. One model points out the existence of a single orocline, the Cantabrian orocline, defining a C-shape, continental-scale single bend [33–35]. In the second model, two oroclines are considered, as follows: a clear northern curvature, namely the Cantabrian Arc (or Cantabrian orocline) [36] and an opposite slightly defined southern curvature, named as the Central Iberian Arc (or Central Iberian Orocline) [37–39]. In this model, the Cantabrian and the Central Iberian arcs define an S-shaped orogenic belt [40–45].

Regardless of the model under consideration, three main compression ductile deformation phases, namely C1, C2, and C3, have been identified in NW Iberia within the GTMZ and CIZ regions [46–49].

C1 and C2 are responsible for the intense Variscan crustal growth. C3, the last Variscan compression, produced vertical folds with a sub-horizontal axis, as well as both subvertical dextral and sinistral strike–slip shear zones.

Hildenbrand et al. [49], based on new K–Ar and 40Ar/39Ar age data combined with previous U–Pb age data from Portuguese granites besides the three main phases of compression (C1, C2, and C3), propose an additional two extensional events (E1 and E2), under given metamorphic conditions and concomitant igneous events (I1 to I3), being considered responsible for the main structures presently observed in the NW Iberia (e.g., [49,50]).

4. Variscan Magmatism

In NW Iberia, large volumes of mafic to felsic magmas were generated and emplaced into Neoproterozoic to Paleozoic metasedimentary and metaigneous sequences. The C3 ductile phase is commonly employed as the reference for classifying the granitic rocks from Central and Northern Portugal, with the ones younger than 305 Ma being considered as post-collisional [51–56].

Grounded in their geologic, petrographic, and geochemical characteristics, granite bodies have been divided into two main groups (e.g., [51,57–59]). The first group consists of two-mica peraluminous granites, resulting from the mesocrustal anatexis of pelitic metasediments with magmatic andalusite, sillimanite, zircon, monazite, and apatite, with frequent metasedimentary enclaves, whose origin at the mid-crustal level is related to orogenic metamorphism. The granites belonging to this group are considered as S-type, according to the classification of Chappell and White [60], are mainly syn-C3, and are usually emplaced in the nucleus of regional C3 folds. The second group consists of biotite-rich granites frequently having mafic magmatic enclaves, representing the products of complex lower-crustal melting with a possible mixture with mantle-derived magmas, and have their emplacement mainly controlled by NW–SE to ENE–WSW shear zones or by late-Variscan tectonic structures (e.g., [52,61,62]).

Considering the relation between the Variscan magmatism and tectonics, the granites from the CIZ and GTMZ can be subdivided into two main groups, as follows: one group related to the I2 event comprising granites crystallized between 330 Ma and 305 Ma, and another group related to the I3 event, corresponding to the granites that crystallized after 305 Ma [49].

The I2 magmatic event includes biotite granites related to the first extension (E1) (ca. 330–315 Ma) controlled by NW–SE to ENE–WSW deep crustal shear zones, and also two-mica granites crystallized between 315 and 305 Ma, usually emplaced in the core of regional C3 folds. The I3 magmatic event includes biotite granites and their differentiated facies, crystallized after 305 Ma, that are mostly isotropic (no macroscopic ductile foliation or lineation), and have their emplacement during/after the final collapse of the Variscan orogeny (E2) [49].

5. AMS Data Integration

5.1. Studied Granite Plutons

Nineteen Variscan granite plutons, with appropriate available AMS data obtained from 876 sites (6–9 samples per site), spanning the period between 320 Ma and 296 Ma, were evaluated (Figure 3, Table 1). According to the classification of Ferreira et al. [51], revised in Hildebrand et al. [49], these granites are (i) pre-collisional: Borralha pluton; (ii) syn-collisional: S. Mamede, Vila Real-Gralheira, and Porto plutons; and (iii) post-collisional: Castelo Branco, Vieira do Minho, Freixo de Numão, Serra da Estrela (Seia and Covilhã facies), Caria-Vila da Ponte, Valpaços, Capinha, Castro Daire, Lamas de Olo, Vila Pouca de Aguiar, Águas Frias-Chaves, Lavadores-Madalena, Esmolfe-Matança, Penedos, and Monção.

The ages and summary textural description of each granite are shown in Table 1.

Table 1. Summary of the main characteristics of the granites studied. All the ages presented are SHRIMP U-Pb ages obtained from zircons or monazites, except for those marked with *, indicating an approximate age assigned based on field relations, geochemical characteristics, and the age of other similar granites.

Pluton	Granites	Age (Ma)	Mineralogy/Texture	References
Borralha	Borralha	320 *	Medium-to-coarse-grained porphyritic biotite granite	[63,64]
S. Mamede	S. Mamede Vila Verde	310 *	Medium-grained two-mica granite Medium-to-coarse-grained two-mica granite	[19]
Vila Real-Gralheira	Vila Real Minheu-Lagoa Gralheira	311 ± 1	Medium-to-coarse-grained two-mica granite Medium-grained porphyritic two-mica granite Medium-to-coarse-grained two-mica granite	[9,65]
Porto	Porto	311 ± 7	Medium-grained porphyritic two-mica granite	[9,66]
Castelo Branco	Alcains Castelo Branco	310 ± 1	Porphyritic two-mica granite Coarse-grained porphyritic monzogranite	[9,67]
Vieira do Minho	Vieira do Minho Moreira de Rei	310 ± 2 307 ± 3.5	Coarse-grained porphyritic monzogranite Medium-grained porphyritic monzogranite	[68]
Freixo de Numão	Freixo de Numão Frei Tomé	306 ± 2	Medium-to-coarse-grained porphyritic two-mica granite Fine-grained two-mica granite	[64,69,70]
Serra da Estrela	Seia Covilhã	304.1 ± 2.9	Coarse-grained porphyritic biotite granites	[71,72]
Caria-Vila da Ponte	Caria Vila da Ponte	301.2 ± 1.2	Medium-grained porphyritic biotite granite Medium-to-coarse-grained porphyritic biotite granite	[12,73]
Valpaços	Valpaços Lagoas	305 ± 17	Medium-to-coarse-grained porphyritic muscovite-biotite granite Fine-grained muscovite granite	[70,74]
Capinha	Capinha	301 ± 3	Medium-grained two-mica porphyritic granite	[64,75]
Castro de Aire	Calde Alva	294.1 ± 3.5	Coarse-grained porphyritic biotite granites Fine-grained two-mica granite	[72,76]

Table 1. *Cont.*

Pluton	Granites	Age (Ma)	Mineralogy/Texture	References
Lamas de Olo	Lamas de Olo Alto dos Cabeços Barragem	297.19 ± 0.73	Medium-to-coarse-grained porphyritic biotite granite Medium-to-fine-grained porphyritic biotite granite Fine-to-medium-grained biotite porphyritic leucogranite	[13,18,77,78]
Vila Pouca de Aguiar	Pedras Salgadas Vila Pouca de Aguiar	297 ± 14 298 ± 9.1	Medium-to-fine-grained porphyritic biotite granite Medium-to-coarse-grained porphyritic monzogranite	[5,79]
Águas Frias-Chaves	Águas Frias St^{o}. António de Monforte	299 ± 3	Coarse-grained porphyritic biotite granite Medium-grained two-mica granite	[5]
Lavadores-Madalena	Madalena Lavadores	298 ± 11	Medium-to-coarse-grained porphyritic biotite granite Medium-grained porphyritic biotite granite	[80,81]
Esmolfe-Matança	Esmolfe-Matança	298 ± 11 to 298 ± 13	Medium-grained porphyritic biotite granite	[77,82]
Penedos	Penedos	298 *	Medium-grained leucogranite with garnet	[34,63,82]
Monção	Monção	296 ± 3	Coarse-grained porphyritic biotite granite	[83]

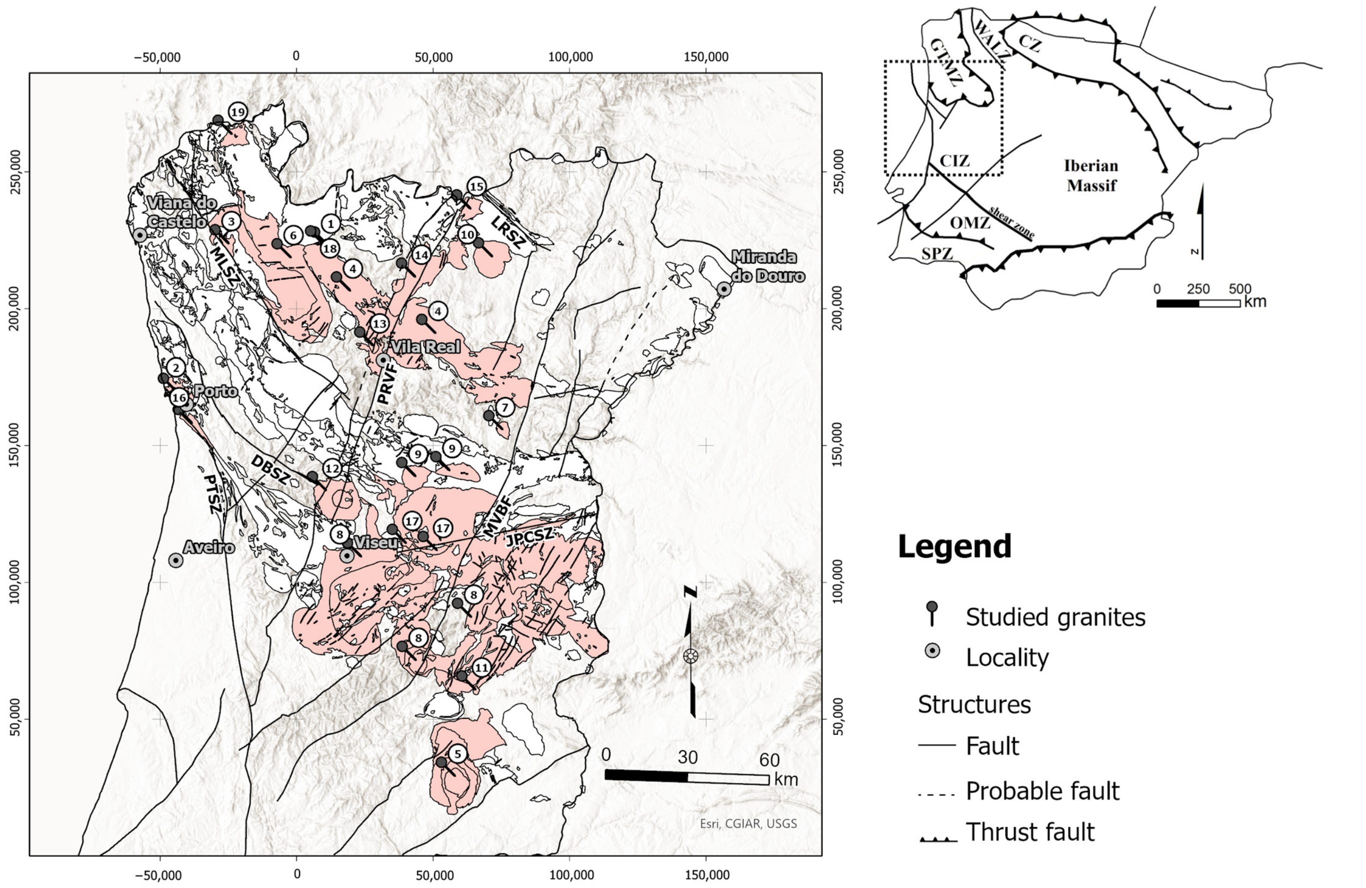

Figure 3. Simplified geologic map of Northern and Central Portugal with the plutons/granites studied (adapted from Ferreira et al. [51]). PTSZ–Porto–Tomar shear zone; MLSZ—Malpica–Lamego shear zone; JPCSZ—Juzbado–Penalva do Castelo shear zone; LRSZ—Laza–Rebordelo shear zone; PRVF—Penacova–Régua-Verín fault; MVBF—Manteigas–Vilariça–Bragança fault. CZ—Cantabrian zone, WALZ—West Asturian-Leonese, GTMZ—Galícia-Trás-os-Montes Zone, CIZ—Central Iberian Zone, OMZ—Ossa-Morena Zone; SPZ—South Portuguese Zone. 1. Borralha; 2. Porto; 3. São Mamede; 4. Vila Real—Gralheira; 5. Castelo Branco; 6. Vieira do Minho; 7. Freixo de Numão; 8. Serra da Estrela (Seia and Covilhã fácies); 9. Caria—Vila da Ponte; 10. Valpaços; 11. Capinha; 12. Castro Daire; 13. Lamas de Olo; 14. Vila Pouca de Aguiar; 15. Águas Frias-Chaves; 16. Lavadores—Madalena; 17. Esmolfe—Matança; 18. Penedos; 19. Monção.

5.2. Variability of Magnetic Susceptibility

A statistical synthesis of the AMS parameters is presented in Table 2. For each pluton, the arithmetic means of the values of Km and P% of each site and their standard deviation were calculated. To determine the magnetic lineation and magnetic foliation of each pluton, mean directions and confidence angles were computed using directional statistics based on the Bingham distribution. The studied Variscan granites exhibit a bulk magnetic susceptibility ranging from 30.4×10^{-6} to $10{,}436.1 \times 10^{-6}$ SI units. In the absence of magnetite, a granite is said to be paramagnetic if its Km value is typically $<400 \times 10^{-6}$ SI (e.g., [26,84]) and its Km is directly correlated with the rock's iron content, according to the Curie–Weiss law [85]. The presence of magnetite, with Km values two orders of magnitude higher for the same amount of iron content compared to paramagnetic minerals, imparts elevated susceptibilities to ferromagnetic granites. Ishihara [86] earlier recognized the bimodal distribution of K values in granites, attributable to the presence or absence of magnetite. In the studied granites, the distribution of magnetic susceptibility values by classes (Table 2 and Figure 4) shows that most granites have a Km lower than 400×10^{-6} SI, showing a paramagnetic behavior, with biotite being the main Fe carrier.

Table 2. Scalar (Km, P%) and vectorial (K1 and K3) parameters with an indication of the average magnetic foliation and lineation; n—number of sampling sites, $\bar{x}$—mean value, σ—standard deviation, d—declination, i—inclination, 95% c.a.—95% confidence angles, n.a.—not available. References given in Table 1.

Pluton		Km ($\times 10^{-6}$ SI) $\bar{x}$	Km ($\times 10^{-6}$ SI) σ	P% $\bar{x}$	P% σ	K1d	K1i	K1 95% c.a.	Magnetic Lineation	K3d	K3i	K3 95% c.a.	Magnetic Foliation
Borralha (n = 7)		53.9	25.8	4.4	1.8	101	5	5	5°/N101°	242	69	3	N152°, 21°NE
S. Mamede (n = 8)		84.2	35.4	4.7	1.12	338	13	23	13°/N338°	16	27	9	N106°, 63°SW
Vila Real-Gralheira (n = 20)		57.2	1.5	3.6	0.5	224	78	10	78°/N224°	38	12	4	N128°, 78°SW
Porto (n = 6)		48.7	3.9	5.9	4.9	128	79	n.a	79°/N128°	13	6	n.a	N103°, 84°SW
Castelo Branco (n = 84)		71.6	28.4	4.6	2.0	137	56	25	56°/N137°	51	2	11	N141°, 88°SW
Vieira do Minho (n = 13)		161.6	37.8	4.2	0.9	147	1	20	1°/N147°	61	27	13	N151°, 63°SW
Freixo de Numão (n = 40)		123.9	23.8	2.6	2.0	112	36	n.a.	36°/N112°	12	37	n.a.	N102°, 53°SW
Serra da Estrela (Seia and Covilhã) (n = 201)		107.0	47.5	4.1	1.1	173	33	43	33°/N173°	267	17	18	N177°, 73°NE
Caria-Vila da Ponte (n = 80)		76.0	15.9	1.8	0.5	340	10	15	10°/N340°	110	62	11	N20°, 28°NW
Valpaços (n = 34)		56.7	10.1	3.1	0.8	110	4	11	4°/N110°	5	63	5	N95°, 27°S
Capinha (n = 30)		73.4	12.3	2.0	1.3	208	8	10	8°/N208°	319	87	3	N59°, 3°SE
Castro Daire (n = 105)		83.0	2.9	3.4	0.9	354	22	46	22°/N354°	253	12	19	N163°, 78°NE
Lamas de Olo (n = 48)		1719.0	6350.6	5.1	2.4	169	28	30	28°/N169°	258	2	14	N168°, 88°NE
Vila Pouca de Aguiar (n = 105)		117.2	40.7	1.3	0.6	359	1	14	1°/N359°	129	83	11	N39°, 7°NW
Águas Frias-Chaves (n = 13)		78.1	22.9	2.1	1.3	296	7	15	7°/N296°	181	80	6	N91°, 10°N
Lavadores-Madalena (n = 14)	Lavadores	10,436.1	2983.6	18.4	4.9	219	78	12	78°/N219°	17	12	9	N107°, 78°SW
	Madalena					98	8	11	8°/N98°	4	16	8	N94°, 74°SW
Esmolfe-Matança (n = 59)		64.4	10.3	3.2	3.7	330	6	8	6°/N330°	110	87	3	N20°, 3°NW
Penedos (n = 6)		30.4	7.0	1.9	2.0	352	44	13	4°/N352°	62	36	6	N152°, 51°SW
Monção (n = 3)		117.4	34.3	1.4	1.5	260	12	n.a	12°/N3260°	153	57	n.a	N63°, 33°NW

When the mean magnetic susceptibility (Km) for each pluton is analyzed, we observe that the class with the highest relative frequency of magnetic susceptibility (32%) is the one ranging between 71×10^{-6} and 90×10^{-6} SI, which corresponds to the granites of S. Mamede, Castro Daire, Castelo Branco, Vila da Ponte, Caria-Vila da Ponte, Capinha, and Águas Frias-Chaves (Figure 4). This class is followed by the one ranging from 51×10^{-6} to 70×10^{-6} SI (21%), corresponding to the granites of Borralha, Porto, Vila Real-Gralheira, Valpaços, Esmolfe-Matança, and Penedos. The class ranging from 91 to 110×10^{-6} SI has 5% of frequency corresponding to Serra da Estrela granites. The classes ranging between

111 × 10^{-6} and 130 × 10^{-6} SI and between 151 × 10^{-6} and 1000 × 10^{-6} SI correspond to Freixo de Numão and Vila Pouca de Aguiar plutons and to Vieira do Minho and Monção plutons, with 16% and 5% frequencies, respectively. In paramagnetic granites, magnetic susceptibility is a useful parameter to distinguish facies in composites massifs, where different facies with variable biotite contents are present, as are the cases of the plutons of Vila Pouca de Aguiar, Águas Frias-Chaves, Serra da Estrela (Seia and Covilhã), Castro Daire, Valpaços, and Castelo Branco.

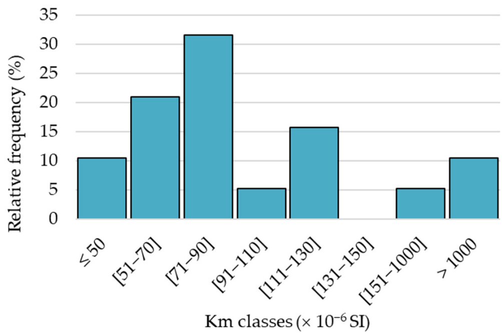

Figure 4. Frequency histogram of mean magnetic susceptibility values for the granites analyzed.

The class with Km > 1000 × 10^{-6} SI corresponds to ferromagnetic granites, which are scarce and are only represented by the Lamas de Olo pluton and the Lavadores-Madalena pluton (Figure 4).

The Lamas de Olo pluton is a composite pluton made up of a main granite facies (Lamas de Olo) with essentially ferromagnetic behavior, indicative of the presence of magnetite, and two other paramagnetic facies (Alto dos Cabeços and Barragem) with a magnetic susceptibility lower than 1000 × 10^{-6} SI [13]. In the ferromagnetic facies, Cruz et al. [13] pointed out that magnetite was partially altered to hematite (martitization), leading to a decrease in the magnetic susceptibility values (Figure 5b,c).

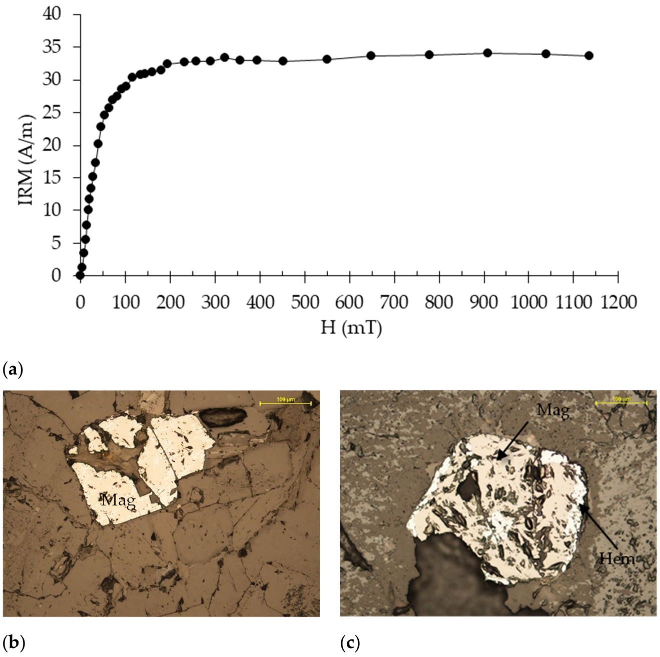

Figure 5. (**a**) Isothermal Remanent Magnetization acquisition curve obtained for Lavadores granite showing the saturation at 300 mT, indicating the presence of magnetite. (**b**,**c**) Reflected light microscopy images showing magnetite (Mg) and hematite (Hem) in the and Lamas de Olo pluton.

The Lavadores-Madalena pluton is composed of Lavadores and Madalena granites, being richer in Lavadores magnetite than Madalena granite, with a magnetic susceptibility mean for both granites of 10,436 $\times$ 10^{-6} SI [80,81].

Confirmation of the existence of ferrimagnetic iron oxide in the Lavadores-Madalena and Lamas de Olo plutons was achieved through Isothermal Remanent Magnetization curves. Additionally, the presence of magnetite was identified in both plutons using reflected light microscopy (Figure 5).

5.3. Magnetic Anisotropy, Field Observations, and Microstructures

Magnetic anisotropy (P%) can be used as a "marker" for the deformation experienced by granite mushes during their crustal emplacement and further cooling. Magnetic anisotropy, recorded using mineral fabrics, can thus be correlated with finite deformation.

In the Variscan granites studied, the magnetic anisotropy ranges between 1.3% and 5.9% (Lavadores-Madalena and Lamas de Olo pluton are not included) and decreases when granites change from being syn-collisional, ages ranging between 320 and 305 Ma, (P = 4.7%) to being post-collisional, ages < 305 Ma (P = 2.9%) (Table 2).

In paramagnetic granites (i.e., where magnetite is absent), magnetic anisotropy is essentially due to iron-rich silicate minerals with a strong crystalline anisotropy, such as biotite. For the plutons where magnetite is present (Lavadores-Madalena and Lamas de Olo plutons), magnetic anisotropy is strongly influenced by the shape anisotropy of the magnetite grains, which is responsible for the high average P% values (18.4% in Lavadores-Madalena pluton and 5.1% in Lamas de Olo plutons). For those ferromagnetic granites, even though a noticeable tectonic deformation may be absent, they exhibit notably higher average P% values.

The magnetic anisotropy of paramagnetic granites can be related to the field observation of the granite fabric at the outcrop scale. Granites that are anisotropic in the field, with a visible orientation of biotite and/or K-feldspars, always have magnetic anisotropies higher than 3%, while granites with anisotropies lower than 2% are isotropic in field observations (Figure 6).

(**a**) (**b**) (**c**)

Figure 6. Outcrop scale photos of selected granites. (**a**) Caria-Vila da Ponte pluton, P = 1.8%; (**b**) Freixo de Numão pluton, P = 2.6%; and (**c**) Valpaços pluton; P = 3.1%. The dashed line marks the orientation of the feldspars or biotites measured in the field.

In addition to the evaluation of magnetic anisotropy, microstructures in granitic rocks must be examined in detail to reconstruct the emplacement process. Microstructures in granitic rocks, mainly in quartz and biotite grains, can be magmatic or low-to-high-temperature solid-state formed.

Magmatic-to-submagmatic microstructures are characterized by a rare undulatory extinction in quartz, scarce subgrain boundaries in quartz, and, eventually, folded or kinked biotites. High-to-medium-temperature solid-state deformation microstructures are characterized by polygonal-shaped quartz subgrains, recrystallized quartz grains, kinked biotites, and, eventually, bands of quartz surrounded by mica flakes.

Figure 7 shows some of the microstructures present in the paramagnetic granites studied, highlighting the different degrees of magmatic and post-magmatic deformation which can be related to magnetic anisotropy.

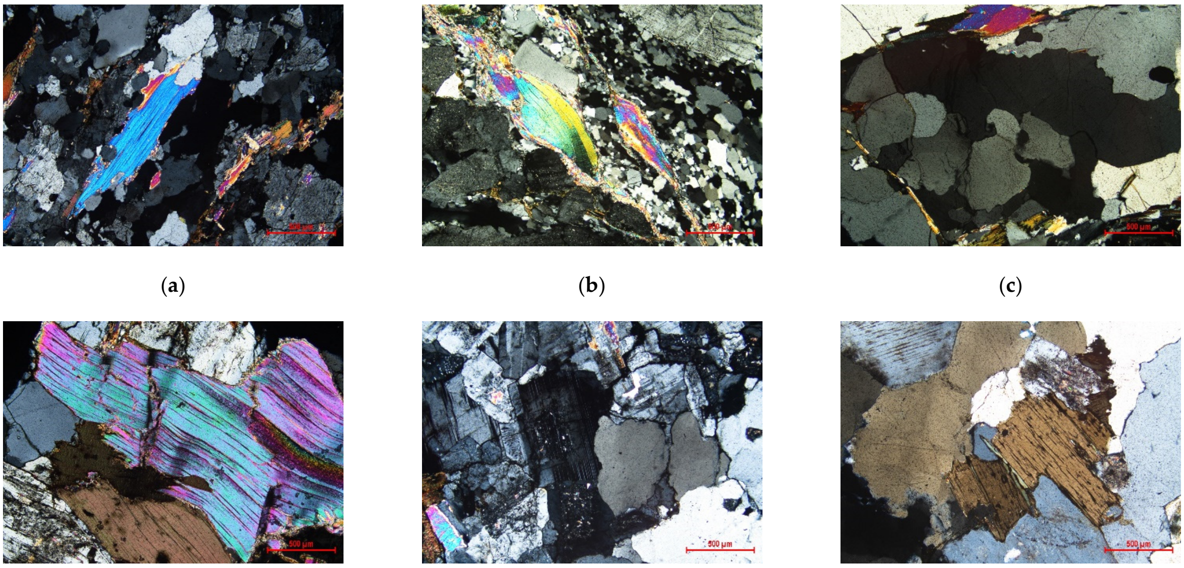

(**a**) (**b**) (**c**)

(**d**) (**e**) (**f**)

Figure 7. Typical microstructures of selected granites: (**a**) Porto pluton, P = 5.9%; (**b**) Castro Daire pluton, P = 5.9%; (**c**) Vila Real-Gralheira pluton, P = 3.6%; (**d**) Castelo Branco pluton P = 4.6%; (**e**) Vila Pouca de Aguiar pluton, P = 1.4%; and (**f**) Vila Pouca de Aguiar pluton, P = 1.0%. All photomicrographs are under crossed polars, scale bar correspond to 500 µm.

Plutons such as the Porto pluton and some samples of the Castro Daire pluton show low-temperature solid-state deformation microstructures (recrystallization of quartz into small grains and an incipient gneissic structure) and have magnetic anisotropy values between 5% and 6% (Figure 7a,b). Plutons like the Castelo Branco and the Vila Real-Gralheira plutons display magmatic-to-high-temperature solid-state deformation microstructures (e.g., kinked biotites and chess-board quartz extinction) and present magnetic anisotropy values around 3 to 5% (Figure 7c,d). Finally, plutons with a deformation hardly visible to the naked eye, such as the Vila Pouca de Aguiar pluton, display a magnetic anisotropy value around 1.5% and exhibit almost ubiquitous magmatic-to-submagmatic microstructures (undeformed biotite, no/rare undulatory extinction, and no subgrains in quartz) (Figure 7e,f).

In the ferromagnetic granites, a high magnetic anisotropy value is not directly related to the intensity of strain that the magma experienced. Instead, it is attributed to the high shape anisotropy of magnetite. The Lavadores-Madalena and Lamas de Olo plutons often present rough alignments of magnetite co-existing with magmatic-to-submagmatic microstructures.

5.4. Magnetic Fabric and Magmatic Strain

The AMS fabric axes tend to be parallel to those of the finite strain undergone by the magma, provided that the strain path is simple [7,87]. Thus, the AMS axes are related to the strain field present during the final stages of magma crystallization [88]. This strain generates the AMS fabric, where the magnetic lineation (K1) coincides with the maximum extension direction (e_1), and the magnetic foliation is perpendicular to the maximum shortening direction (e_3) [89,90]. Magnetic foliations and lineations approximate the flattening plane and the stretching axis of the finite strain ellipsoid.

The AMS fabric can be a result of (1) the magmatic flow during emplacement, including stress applied by the ascending magma column on the melt (e.g., [91–93]); (2) regional tectonic stress during emplacement and crystallization (e.g., [94–96]); or (3) a combination of both (e.g., [97]). During emplacement, the intrusion may record multiple fabrics, which can be progressively replaced [88] or overprinted [97] when the stress conditions change. When the melt finally approaches the solidus, it is the youngest fabric that is registered.

The set of granitic intrusions whose genesis is related to an orogenic process, such as the Variscan granitic plutons studied, will register several AMS fabrics as the result of the strain that affected the plutons, expressing the evolution of the stress field during the orogeny.

The extensive homogeneity of the AMS fabrics within plutons has been consistently confirmed in various studies, particularly through the examination of foliation and magnetic lineation maps, especially in the context of paramagnetic granites (e.g., [84] and references therein). Olivier et al. [98] demonstrated that granites exhibit a remarkably consistent fabric, observable from the scale of the individual samples to that of an entire pluton. The structural consistency observed in granites indicates that the magma reservoirs, as they intrude the crust, undergo a uniform deformation process before crystallization, as demonstrated by previous research (e.g., [84]).

The magnetic fabric within the studied plutons also displays a notable uniformity. However, it is evident that the magnetic foliation consistently exhibits a clearer definition compared to the magnetic lineation, as indicated by the confidence angle values of K1 and K3, presented in Table 2. This difference may be attributed to the fact that, in most plutons, magnetic foliation results from the planar distribution of biotite cleavage planes. Regarding lineation, it tends to exhibit variations depending on its relative position within the pluton, with, for instance, a tendency to be more vertical in the root zone.

Except for the S. Mamede, Penedos, and Freixo de Numão plutons, the fabric's uniformity permits the use of the mean values of lineation and magnetic foliation as being representative of the entire pluton.

Burton-Johnson et al. [89,90] considered that when the AMS fabrics record magmatic tectonic strain, the strain axes (the maximum extension direction, e_1, the intermediate, e_2, and the minimum, e_3) relate to the tectonic stress axes that affect the granitic magma (the maximum compression direction, σ_1, the intermediate, σ_2, and the minimum, σ_3) (Figure 8).

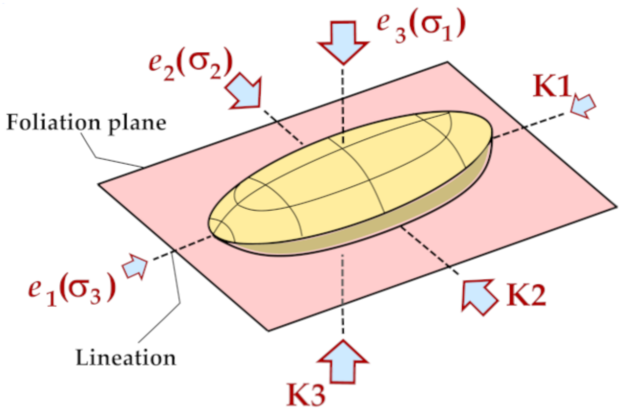

Figure 8. Under coaxial, non-rotational shear, the minimum extension direction (e_3) is parallel to K3 and to the direction of maximum compressive stress, σ1, whilst the maximum extension (e_1) will be parallel to K1 and to the direction of minimum compressive stress, σ3 (adapted from Burton-Johnson et al. [89,90]).

Burton-Johnson et al. [89] compared the AMS axes with the tectonic deformation axes for various plutons worldwide in both compressional and extensional regimes, showing that during high tectonic compression, sub-horizontal tectonic compression is the dominant stress (σ_1) and the subvertical lithostatic compression is the weakest stress (σ_3). Thus, under coaxial pure shear, the foliation pole (e_3 and K3) is sub-horizontal (parallel to σ_1) and the lineation direction (e_1 and K1; parallel to σ_3) is subvertical. On the other hand, during extension, subvertical lithostatic compression is σ_1, and the direction of crustal extension is σ_3. In this case, K3 (e_3) is subvertical and K1 (e_1) is sub-horizontal, in the direction of extension.

These authors considered an intermediate tectonic pure shear regime reflecting moderate tectonic compression, as follows: if the tectonic compression σ_1 is sub-horizontal and the subvertical lithostatic compression is σ_2, then both K1 and K3 are sub-horizontal.

Applying these insights, the K1 (Kmax) and K3 (Kmin) fabric data were analyzed for each of the plutons studied, considering the relationship between the magnetic lineation and the pole (normal) of the magnetic foliation and the directions of minimum and maximum compressive stress, respectively (Figure 9). In the case of S. Mamede, Penedos, and Freixo de Numão plutons, this analysis was not carried out because the axes of the AMS ellipsoid were too scattered to perform the statistical determination of the K1, K2, and K3 means. Figure 9 shows the K1 and K3 stereoplots for each granite pluton, their orientation description, the summarized description of the AMS lineation and foliation, and the emplacement tectonic setting interpretation.

Based on the synthesis presented in Figure 9, we can hypothesize that the studied plutons were emplaced in the following three tectonic regimes:

(i) Plutons emplaced during high compression (pure shear)

In this case, the high degree of tectonic compression, σ_1, is sub-horizontal and the subvertical compression is σ_3. The foliation pole (e_3 and K3) is sub-horizontal (parallel to σ_1), the magnetic foliation is subvertical, and the magnetic lineation direction (e_1 and K1; parallel to σ_3) is subvertical. These are the cases of Porto (311 $\pm$ 7 Ma), Vila Real-Gralheira (311 $\pm$ 1 Ma), and Castelo Branco pluton (310 $\pm$ 1 Ma), where the magnetic foliations are vertical, with a general NW–SE trend; the magnetic lineations are subvertical; and the shortening direction is horizontal, with a NE–SW direction.

(ii) Plutons emplaced during moderate compression level (pure shear)

In this case, the tectonic compression σ_1 is sub-horizontal with σ_2, subvertical, and both K1 and K3 are sub-horizontal, and the magnetic foliation is subvertical. These are the cases of the Vieira do Minho (310 $\pm$ 2 Ma to 307 $\pm$ 3.5 Ma), Serra da Estrela (Seia and Covilhã) (304.1 $\pm$ 2.9 Ma), Castro Daire (294.1 $\pm$ 3.5 Ma), and Lamas de Olo plutons (297.19 $\pm$ 0.73 Ma). These suites have vertical magnetic foliations, NNW–SSE trending due to a ENE–WSW to E–W horizontal compression.

(iii) Plutons emplaced during extension (pure shear)

In this case, σ_1 is subvertical and the direction of the crustal extension is σ_3. The foliation pole defined by e_3 (K3) is subvertical, the magnetic foliation is horizontal, and e_1 (K1) is sub-horizontal in the direction of extension. These are the cases of the Borralha, Caria-Vila da Ponte, Valpaços, Capinha, Vila Pouca de Aguiar, Águas Frias-Chaves, Esmolfe-Matança, and Monção plutons. In the Borralha (320 Ma), Caria-Vila da Ponte (301.2 $\pm$ 1.2 Ma), Valpaços (305 $\pm$ 17 Ma), Capinha (301 $\pm$ 3 Ma), Vila Pouca de Aguiar (297 $\pm$ 14 Ma), Águas Frias-Chaves (299 $\pm$ 3 Ma), Esmolfe-Matança (298 $\pm$ 11 to 298 $\pm$ 13 Ma), and Monção plutons (296$\pm$ 3 Ma), the magnetic foliations are horizontal/sub-horizontal and the main tectonic compression is vertical. The magnetic lineations are horizontal/sub-horizontal. The magmatic stretching (K1 direction) is NW–SE in the Borralha, Caria-Vila da Ponte, Valpaços, Vila Pouca de Aguiar, Águas Frias-Chaves, and Esmolfe-Matança plutons. It trends in the NE–SW and E–W directions in the Capinha and Monção plutons, respectively.

The Lavadores-Madalena pluton is discussed separately as it has two granitic facies, Lavadores and Madalena, with different magnetic fabrics (Figure 9). The foliation pole (K3) is sub-horizontal, the magnetic foliation is WNW–ESE, subvertical, and the magnetic lineation direction (K1) is subvertical. Thus, σ_1 is sub-horizontal and the subvertical compression is σ_3. In Madalena facies, both K1 and K3 are sub-horizontal and the magnetic foliation is E–W subvertical, indicating that σ_1 is sub-horizontal and that lithostatic compression, σ_2, is vertical.

Pluton	K1 (lineation)	K3 (pole of foliation)	Stereoplots descriptions	AMS fabric	Emplacement tectonic setting interpretation
Borralha	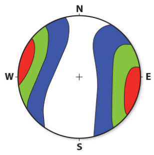	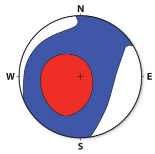	K1 orientations define a sub–horizontal cluster, directed ESE–WNW. K3 orientations define an approximate NE–SW girdle, with a poorly defined subvertical cluster.	Horizontal lineation. Sub–horizontal foliation.	σ1 subvertical. Subvertical compression. Extensional.
Vila Real–Gralheira	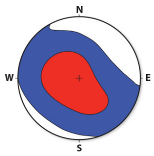	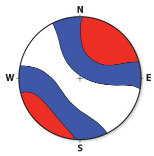	K1 orientations with a poorly defined subvertical cluster. K3 orientations define a sub–horizontal cluster, directed NE–SW.	Subvertical lineation. Subvertical NW–SE foliation.	σ3 subvertical. NE–SW horizontal compression.
Porto	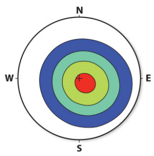	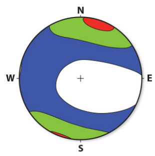	K1 orientations define a vertical cluster. K3 orientations define a sub–horizontal cluster, directed NNE–SSW.	Subvertical lineation. Vertical WNW–ESE foliation.	σ3 vertical. NNE–SSW horizontal compression.
Castelo Branco	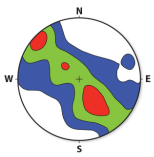	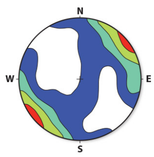	K1 orientations define an approximate NW–SE girdle, with a poorly defined subvertical cluster. K3 orientations define a sub–horizontal cluster, directed NE–SW.	Subvertical lineation. Subvertical NW–SE foliation.	σ3 subvertical. NE–SW horizontal compression.
Vieira do Minho	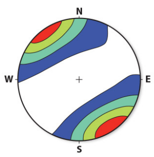	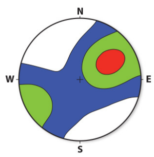	K1 orientations define a sub–horizontal cluster, directed NNW–SSE. K3 orientations define an approximate NE–SW girdle.	Horizontal lineation. Subvertical NW–SE foliation.	σ2 subvertical. NE–SW horizontal compression. NNW–SSE strike–slip fault.
Serra da Estrela	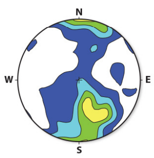	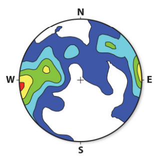	K1 orientations define a sub–horizontal to intermediate cluster, directed N–S. K3 orientations define a sub–horizontal cluster, directed ENE–WSW.	Sub–horizontal lineation. Subvertical NNW–SSE foliation.	σ2 subvertical. ENE–WSW horizontal compression. NNW–SSE strike–slip fault.

Figure 9. *Cont.*

Pluton	K1 (lineation)	K3 (pole of foliation)	Stereoplots descriptions	AMS fabric	Emplacement tectonic setting interpretation
Caria–Vila da Ponte	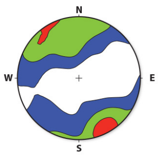	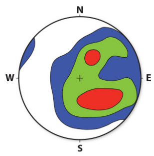	K1 orientations define a sub–horizontal cluster, directed NW–SE. K3 orientations define a poorly defined subvertical cluster.	Sub–horizontal lineation. Sub–horizontal foliation.	σ1 subvertical. Subvertical compression. Extensional.
Valpaços	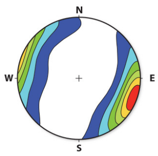	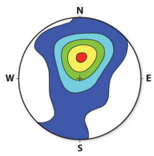	K1 orientations define a sub–horizontal cluster, directed WNW–ESE. K3 orientations define a subvertical cluster.	Horizontal lineation. Sub–horizontal foliation.	σ1 subvertical. Subvertical compression. Extensional.
Capinha	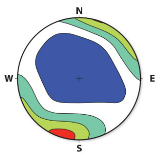	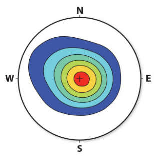	K1 orientations define a poorly defined sub–horizontal cluster, directed NE–SW. K3 orientations define a vertical cluster.	Horizontal lineation. Horizontal foliation.	σ1 subvertical. Subvertical compression. Extensional.
Castro Daire	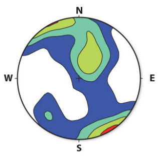	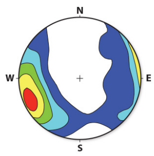	K1 orientations define a sub–horizontal cluster, directed NW–SE. K3 orientations define a sub–horizontal cluster, directed ENE–WSW.	Sub–horizontal lineation. Subvertical NNW–SSE foliation.	σ2 subvertical. ENE–WSW horizontal compression. NNW–SSE strike–slip fault.
Lamas de Olo	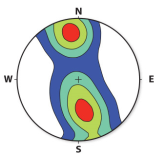	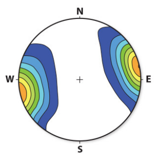	K1 orientations define an approximate NNW–ESE girdle, with two sub–horizontal to intermediate clusters. K3 orientations define a sub–horizontal cluster, directed ENE–WSW.	Two sub–horizontal to intermediate lineations. Vertical NNW–SSE foliation.	σ2 subvertical. ENE–WSW horizontal compression. NNW–SSE strike–slip fault.
Vila Pouca de Aguiar	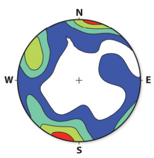	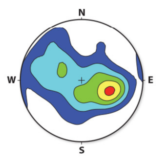	K1 orientations define a sub–horizontal cluster, directed NNW–SSE. K3 orientations define a subvertical cluster.	Horizontal lineation. Horizontal foliation.	σ1 subvertical. Subvertical compression. Extensional.

Figure 9. *Cont.*

Pluton	K1 (lineation)	K3 (pole of foliation)	Stereoplots descriptions	AMS fabric	Emplacement tectonic setting interpretation
Águas Frias–Chaves	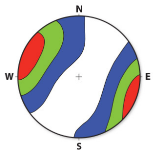	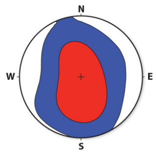	K1 orientations define a sub–horizontal cluster, directed ESE–WNW. K3 orientations define a poorly defined subvertical cluster.	Horizontal lineation. Sub–horizontal foliation.	σ1 subvertical. Subvertical compression. Extensional.
Lavadores–Madalena Lavadores	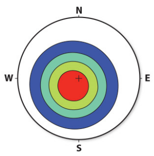	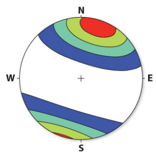	K1 orientations define a vertical cluster. K3 orientations define a sub–horizontal cluster, directed NNE–SSW.	Subvertical lineation. Subvertical WNW–ESE foliation.	σ3 vertical. NNE–SSW horizontal compression.
Madalena	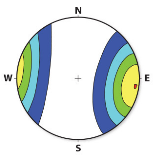	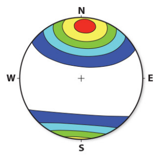	K1 orientations define a sub–horizontal cluster, directed E–W. K3 orientations define a sub–horizontal cluster, directed N–S.	Horizontal lineation. Subvertical E–W foliation.	σ2 subvertical. N–S horizontal moderate compression.
Esmolfe–Matança	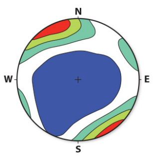	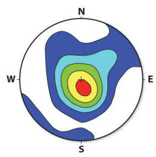	K1 orientations define a sub–horizontal cluster, directed NNW–SSE. K3 orientations define a subvertical cluster.	Horizontal lineation. Horizontal foliation.	σ1 subvertical. Vertical compression. Extensional.
Monção	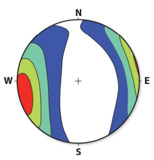	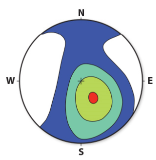	K1 orientations define a sub–horizontal cluster, directed ESE–WNW. K3 orientations define a subvertical cluster.	Horizontal lineation. Sub–horizontal foliation.	σ1 subvertical. Subvertical compression. Extensional.

Figure 9. Synthesis of magnetic lineation (K1) and pole to magnetic foliation (K3) stereos for the plutons considered. Schmidt, lower hemisphere projections, Kamb contours. Color gradient—blue to red—representing density of points per area. The references for the ages of the plutons are given in Table 1. The number of sites for each pluton is given in Table 2.

6. Understanding the Magmatic History of the Iberian Variscan: AMS Contribution

6.1. Pluton Classification Using Tectonic Emplacement Settings

The tectonic settings established for the plutons' emplacement were correlated to the estimated ages for the granitic plutons (Figure 10). In this approach, the Lavadores-Madalena pluton was not considered and is discussed separately.

This chronologic analysis enables the identification of a magmatic event within the time frame of 330–315 Ma, occurring in an extensional regime (E1). The Borralha pluton serves as an illustrative example, recording an extensional AMS fabric and is, therefore, considered a syn-E1 granite.

However, most of the plutons studied are related to magmatic events that occurred during Variscan collision (C3), in a compressional tectonic regime between 315 and 305 Ma and are, therefore, considered as syn-C3 granites.

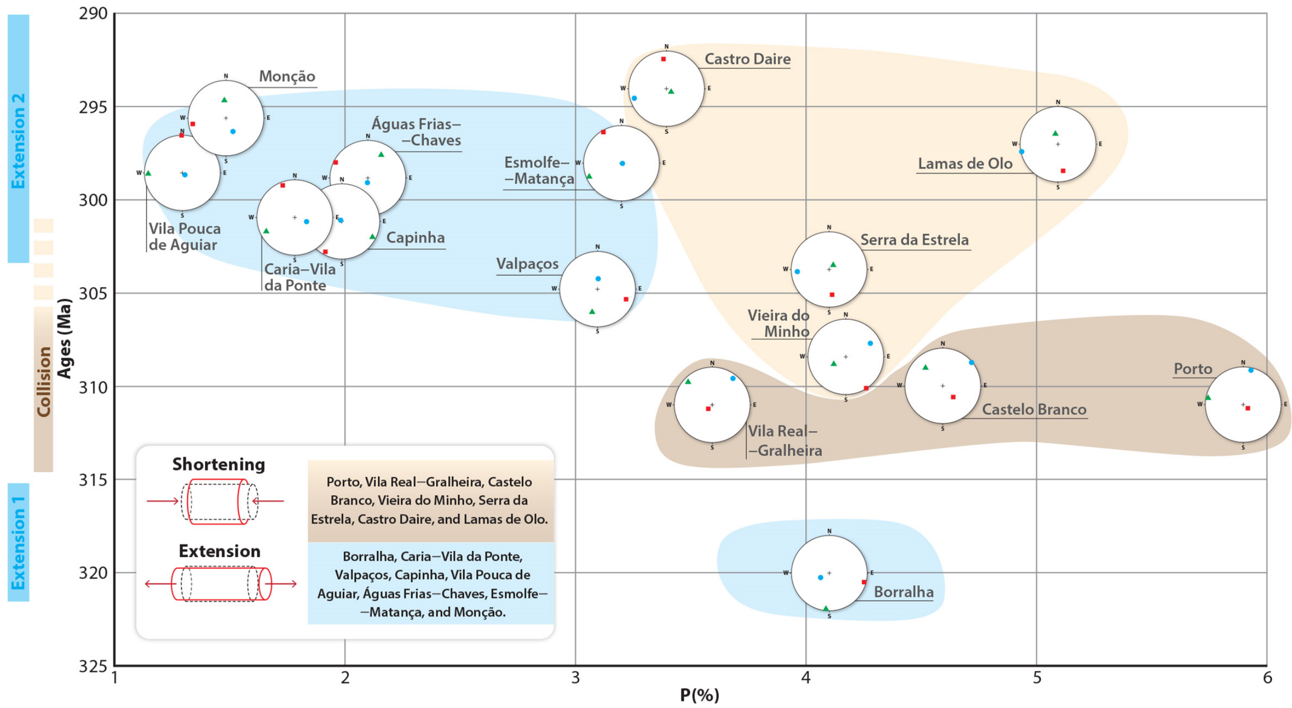

Figure 10. Comparison between the pluton AMS fabrics according to their ages and tectonic emplacement regimes. In the AMS stereos: red square, Kmax; green triangle, Kint; and blue circle, Kmin.

The plutons emplaced during this age interval (namely, Porto, Vila Real-Gralheira, and Castelo Branco) record vertical NW–SE magnetic foliations and vertical lineations, indicating an horizontal NE–SW high tectonic compression (Figure 10). It is worth mentioning that these plutons display clear macroscopic and microscopic fabric.

The plutons younger than 305 Ma were emplaced in tectonic settings changing from a moderately compressive regime to an extensional one. Serra da Estrela, Vieira do Minho, Castro Daire, and Lamas de Olo are examples of plutons emplaced during an ENE–WSW horizontal compression in the late stages of collision. The magnetic foliations of these plutons recorded an emplacement controlled by regional late-C3, NNW–SSE strike–slip faults in a wrench regime.

With the end of the collision, the tectonic setting evolved to an extensional regime (E2), during which the Caria-Vila da Ponte, Valpaços, Capinha, Vila Pouca de Aguiar, Águas Frias-Chaves, Esmolfe-Matança, and Monção plutons were emplaced (Figure 10). Thus, this set of granites is considered as syn-E2 granites.

Concerning the Lavadores-Madalena pluton, with an age of 298 ± 11 Ma, the emplacement took place in a more complex tectonic setting. In the Lavadores facies, K1 is vertical (σ_3 vertical) and in the Madalena facies, K1 is horizontal. However, the samples of Lavadores facies were collected over a very small area [80] when compared with the ones from the Madalena facies, in which the samples cover a larger exposure of the pluton [81]. The authors of [79] interpret the location where the samples of Lavadores facies were collected as the feeding zone of the pluton supporting the subvertical lineations. In the Madalena facies, σ_2 is vertical, compatible with an emplacement in a strike–slip fault. Sant'Ovaia et al. [81] interpreted the magnetic fabric of the Lavadores-Madalena pluton as being acquired in a magmatic state controlled by fractures associated with the main regional structure, i.e., the Porto–Tomar shear zone (represented in Figure 1).

6.2. *Magnetic Susceptibility and Magnetic Anisotropy Geologic Meaning*

The assessment of Variscan granites, particularly in terms of biotite and/or muscovite content (biotite-rich vs. two-mica granites), holds significant importance as it can be linked to the nature of mineralization associated with these granites. In the CIZ, Sn-W mineralizations are commonly linked to paramagnetic, peraluminous two-mica granites. Conversely, W-Mo mineralizations tend to occur in association with biotite granites containing magnetite (e.g., [99,100]). Thus, the distinction between these types of granites is crucial, with Km playing a key role in identifying them.

Sant'Ovaia and Noronha [101] established a classification for Variscan granites based on their magnetic susceptibility (Km) and magnetic anisotropy. The authors considered a Km value of 70×10^{-6} SI as the boundary between granites with muscovite content equal or higher than biotite and granites with biotite higher than muscovite. The integration of additional AMS data makes it possible to refine this boundary. The relation between Km and P% is presented in Figure 11. Considering the biotite vs. muscovite contribution of the studied granites (Table 1), the two-mica (muscovite > biotite) granites have magnetic susceptibility values ranging between 30×10^{-6} and 70×10^{-6} SI, which are lower than the values displayed by the biotite-rich facies (biotite > muscovite), with magnetic susceptibility values higher than 110×10^{-6} SI. The composite plutons, with both facies, have magnetic susceptibility values ranging between 70×10^{-6} and 110×10^{-6} SI.

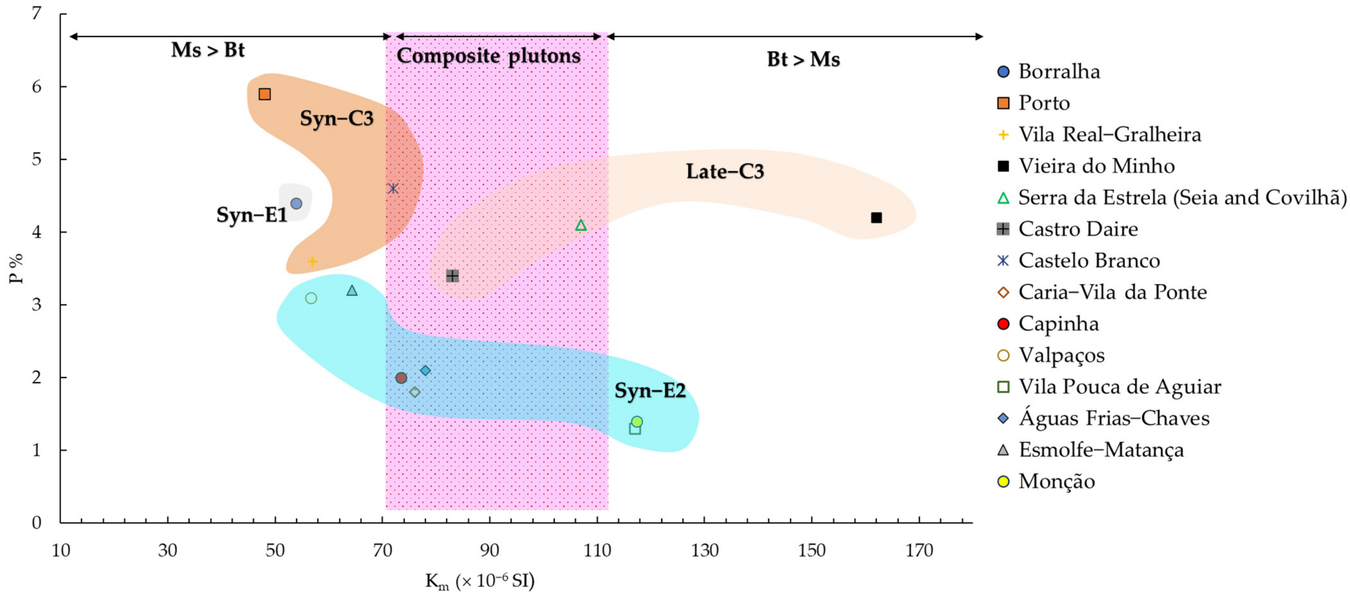

Figure 11. Relationship between the Km and P% parameters for the studied paramagnetic Variscan granites (Sant'Ovaia and Noronha [101], modified). Lavadores-Madalena, Lamas de Olo, Freixo de Numão, Penedos, and S.Mamede were not included.

The syn-C3 plutons have a Km ranging from 49×10^{-6} to 72×10^{-6} SI (Figure 11) and include granites containing biotite and primary muscovite The variation in the relative amounts of biotite and muscovite within the plutons contributes to the dispersion of Km values, reflecting its compositional differences. The emplacement of these plutons during the C3 phase is reflected in the range of magnetic anisotropies between 3.6 and 5.9%.

Late stage-C3 plutons with Km values between 83×10^{-6} and 162×10^{-6} SI are represented by composite plutons having biotite granite facies with calcium plagioclase with different degrees of deuteric alteration. Such post-magmatic alterations produce a decrease in Fe, mainly due to biotite alteration and crystallization of secondary muscovite, implying a decrease in Km values. The emplacement of these plutons in moderate compression settings is reflected in their magnetic anisotropy ranging between 3.4 and 4.2% (Figure 11).

Syn-E2 plutons are also mainly represented by biotite granites with calcium plagioclase with Km values between 57×10^{-6} and 117×10^{-6} SI and a magnetic anisotropy always lower than 3.3% (Figure 11).

Both late-C3 and syn-E2 granites represent the products of complex lower crustal melting with possible mixture with mantle-derived magmas [49].

As was already discussed, magnetic susceptibility values can give information about magnetic mineralogy, namely the presence/absence of magnetite, which is very important to understand the magma redox conditions.

The significance of the paramagnetic or ferromagnetic (s.l.) behavior of granites was the basis of the classification of Ishihara [86]. This author recognized that the magnetite-series granitoids were relatively oxidized, whereas the ilmenite-series granitoids were relatively reduced, and that both types were associated with distinctive ore deposits. These two series are the result of reactions that remove magnetite (or inhibit its formation) during the crystallization of granitic rocks. Two main processes can control the stability of magnetite in granitic rocks, (1) reduction by combustion of carbon during the melting of metasedimentary rocks [86]; or (2) in reduced rocks, consumption by reactions with the Fe–Mg-bearing silicates [102,103]. Even so, the occurrence of magnetite or ilmenite in granites is primarily controlled by the oxidation state of the source material, but also by the differentiation degree of the granite melt [104].

The dominant paramagnetic behavior of the granite plutons evaluated in this work indicates the significance of biotite as the main ferromagnesian mineral. This trait highlights the reduced conditions involved in granite melt formation during the Variscan orogeny, suggesting a dominant graphite-bearing (i.e., reducing) source for these crustal derived collisional magmas [104].

7. Conclusions

This study consolidates data gathered from over 20 papers and PhD theses on the anisotropy of magnetic susceptibility of 19 granitic bodies, covering the time frame from 320 Ma to 296 Ma. The AMS data are derived from 876 sampling sites, including more than 7080 AMS measurements and, throughout the text, a reassessment is suggested.

The standardized magnetic information, namely magnetic susceptibility, magnetic anisotropy, and the AMS fabric, enabled the initial objectives to be achieved, and the following conclusions can be drawn:

i. The Variscan studied granites exhibit a magnetic susceptibility ranging from 30.4×10^{-6} to $10{,}436.1 \times 10^{-6}$ SI units. The distribution of magnetic susceptibility values by classes shows that granites mostly have Km values lower than 1000×10^{-6} SI, showing a paramagnetic behavior, with the biotite being the main Fe carrier. The two-mica (muscovite > biotite) granites show magnetic susceptibility values ranging between 30×10^{-6} SI and 70×10^{-6} SI, which are lower than the values displayed by the biotite-rich facies (biotite > muscovite), with magnetic susceptibility values higher than 110×10^{-6} SI. The composite plutons, with both facies, have magnetic susceptibility values ranging between 70×10^{-6} SI and 110×10^{-6} SI.

ii. The dominant paramagnetic behavior of the granite plutons studied in this work reflects the presence of biotite as the more important ferromagnesian phase. This feature indicates the reduced conditions involved in the granite melt formation during the Variscan orogeny, suggesting a dominant graphite-bearing (i.e., reducing) source for these collisional magmas. The Lavadores-Madalena pluton, among the granites studied, is the only example of a truly Variscan magnetite-type granite, suggesting a deep magma origin and the presence of melt-oxidized conditions, controlled by the source region.

iii. Magnetic anisotropy fabrics are related to structures observed in the granites at different scales. Granites that are anisotropic in the field, with a visible orientation of biotite and/or K-feldspars and have magnetic anisotropies > 3%, while granites with anisotropies < 2%, are isotropic, based on field observations. Syn to late-C3 granites show essentially high-to-medium-temperature solid-state deformation microstructures with magmatic-to-submagmatic microstructures being less commonly observed. The magnetic anisotropy in these granites exceeds 3.3%. Syn-E2 granites display almost ubiquitous magmatic-to-submagmatic microstructures and a magnetic anisotropy < 3.3%.

iv. The studied set of granitic intrusions shows AMS fabrics that record the stress affecting the granites, expressing the chronologic evolution of the stress status during the orogeny. This chronologic approach highlights the magmatic events occurring between around 330 Ma and 315 Ma, attending an extensional regime. The Borralha pluton serves as an example of a suite that recorded an extensional AMS fabric and is, therefore, considered a syn-E1 granite. Plutons with ages between 315 Ma and 305 Ma show AMS fabrics defining their emplacement in a compressional tectonic regime related to the Variscan collision and can, therefore, be considered as syn-C3 granites. Plutons younger than 305 Ma record AMS fabrics indicating a tectonic setting changing from a wrench regime (late-C3 granites) to an extensional one (syn-E2 granites), at the end of the collision stage. The tectonic wrench and the extensional regimes show some chronological overlap, because plutons of similar ages show AMS fabrics recording extension and moderate compression tectonic settings.

Author Contributions: Conceptualization, H.S.; methodology, H.S., C.C., A.G., P.N. and F.N.; software, H.S., C.C. and A.G.; validation, H.S., C.C., A.G., P.N. and F.N.; formal analysis, H.S., C.C. and A.G.; investigation, H.S., C.C., A.G., P.N. and F.N.; resources, H.S., C.C. and A.G.; data curation, H.S.; writing—original draft preparation, H.S.; writing—review and editing, H.S., C.C., A.G., P.N. and F.N.; visualization, H.S., C.C., A.G., P.N. and F.N.; supervision, H.S.; project administration, H.S.; funding acquisition, H.S. All authors have read and agreed to the published version of the manuscript.

Funding: This work is supported by national funding awarded by the FCT—Foundation for Science and Technology, I.P., projects UIDB/04683/2020 (DOI: 10.54499/UIDB/04683/2020) and UIDP/04683/2020 (DOI: 10.54499/UIDP/04683/2020). C. Cruz is a contracted researcher under the UIDP/04683/2020 project (Fundação para Ciência e a Tecnologia—Portugal).

Data Availability Statement: The raw data supporting the conclusions of this article will be made available by the authors on request.

Acknowledgments: The authors express their sincere gratitude to Vladimir Pavlov and to the anonymous reviewers for their valuable time, expertise, and constructive feedback that significantly contributed to the enhancement of this article. The authors extend their appreciation to Emilio Pueyo and to Luke Wu for their guidance and insightful recommendations throughout the review process.

Conflicts of Interest: The authors declare no conflict of interest.

References

1. Rochette, P. Magnetic susceptibility of the rock matrix related to magnetic fabric studies. *J. Struct. Geol.* **1987**, *9*, 1015–1020. [CrossRef]
2. Bouchez, J.L.; Gleizes, G. Two-stage deformation of the Mont-Louis-Andorra granite pluton (Variscan Pyrenees) inferred from magnetic susceptibility anisotropy. *J. Geol. Soc.* **1995**, *152*, 669–679. [CrossRef]
3. Vigneresse, J.L. Control of granite emplacement by regional deformation. *Tectonophysics* **1995**, *249*, 173–186. [CrossRef]
4. Bouchez, J.L. Granite is never isotropic: An introduction to AMS studies of granitic rocks. In *Granite: From Melt to Emplacement Fabrics*; Bouchez, J.L., Hutton, D.H.W., Eds.; Kluwer Academic Publishers: Dordrecht, The Netherlands, 1997; pp. 95–112.
5. Martins, H.C.B.; Sant'Ovaia, H.; Noronha, F. Genesis and emplacement of felsic Variscan plutons within a deep crustal lineation, the Penacova-Régua-Verín fault: An integrated geophysics and geochemical study (NW Iberian Peninsula). *Lithos* **2009**, *111*, 142–155. [CrossRef]
6. Hrouda, F. Modelling Relationship between Bulk Susceptibility and AMS in Rocks Consisting of Two Magnetic Fractions Represented by Ferromagnetic and Paramagnetic Minerals—Implications for Understanding Magnetic Fabrics in Deformed Rocks. *J. Geol. Soc.* **2010**, *75*, 254–266. [CrossRef]
7. Borradaile, G.J.; Jackson, M. Structural geology, petrofabrics and magnetic fabrics (AMS, AARM, AIRM). *J. Struct. Geol.* **2010**, *32*, 1519–1551. [CrossRef]
8. Saint-Blanquat, M.; Law, R.D.; Bouchez, J.L.; Morgan, S. Internal structure and emplacement of the Papoose Flat pluton: An integrated structural, petrographic and magnetic susceptibility study. *Geol. Soc. Am. Bull.* **2001**, *113*, 976–995. [CrossRef]
9. Sant'Ovaia, H.; Martins, H.C.B.; Noronha, F. Oxidized and reduced Portuguese Variscan granites associated with W and Sn hydrothermal lode deposits: Magnetic susceptibility results. *Com. Geol.* **2013**, *100*, 33–39.
10. Porquet, M.; Pueyo, E.L.; Róman-Berdiel, T.; Olivier, P.; Longares, L.A.; Cuevas, J.; The Geokin3DPyr Working Group. Anisotropy of magnetic susceptibility of the Pyrenean granites. *J. Maps* **2017**, *13*, 438–448. [CrossRef]

11. Valle Aguado, B.; Azevedo, M.R.; Nolan, J.; Medina, J.; Costa, M.M.; Corfu, F.; Martínez Catal'an, J.R. Granite emplacement at the termination of a major Variscantranscurrent shear zone: The late collisional Viseu batholith. *J. Struct. Geol.* **2017**, *98*, 15–37. [CrossRef]
12. Gonçalves, A.; Sant'Ovaia, H.; Noronha, H. Emplacement mechanism of Caria-Vila da Ponte Pluton (Northern Portugal): Building and internal magmatic record. *J. Struct. Geol.* **2019**, *124*, 91–111. [CrossRef]
13. Cruz, C.; Sant'Ovaia, H.; Noronha, F. Magnetic mineralogy of Variscan granites from northern Portugal: An approach to their petrogenesis and metallogenic potential. *Geol. Acta* **2020**, *18*, 1–20. [CrossRef]
14. Aranguren, A. Magnetic fabric and 3D geometry of the Hombreiro-Sta. Eulalia pluton: Implications for the Variscan structures of eastern Galicia, NW Spain. *Tectonophysics* **1997**, *273*, 329–344. [CrossRef]
15. Aranguren, A.; Cuevas, J.; Tubía, J.M.; Román-Berdiel, T. Granite laccolith emplacement in the Iberian arc: AMS and gravity study of the La Tojiza pluton (NW Spain). *J. Geol. Soc.* **2003**, *160*, 435–445. [CrossRef]
16. Román-Berdiel, T.; Aranguren, A.; Cuevas, J.; Tubía, J.M. Compressional granite-emplacement model: Structural and magnetic study of the Trives Massif (NW Spain). *Lithos* **1998**, *44*, 37–52. [CrossRef]
17. Román-Berdiel, T.; Aranguren, A.; Casas, A.M.; Urionabarrenechea, J.C.; Pueyo, E.; Tubía, J.M. La lineación magnética en los granitos hercínicos del Noroeste de la Península Ibérica. In *MAGIBER I*; Paleomagnetismo en Iberia (SGE): Burgos, Spain, 2001; pp. 93–100.
18. Cruz, C.; Sant'Ovaia, H.; Raposo, M.I.B.; Lourenço, J.M.; Almeida, F.; Noronha, F. Unraveling the emplacement history of a Portuguese post-tectonic Variscan pluton using fabrics and gravimetry. *J. Struct. Geol.* **2021**, *153*, 104470. [CrossRef]
19. Gonçalves, A.; Sant'Ovaia, H.; Noronha, F. Identification of hydrothermal alteration zones in granitic areas using Magnetic susceptibility, an example in NW Portugal. In Proceedings of the 17th International Multidisciplinary scientific Geoconference, SGEM, Albena, Bulgaria, 29 June–5 July 2017; Volume 17, pp. 383–390. [CrossRef]
20. Julivert, M.; Fontboté, J.M.; Ribeiro, A.; Conde, L. *Mapa Tectónico de la Península Ibérica y Baleares a Escala 1:1.000.000 y Memoria Explicativa*; Instituto Geologico y Mineiro de España: Madrid, Spain, 1974; 113p.
21. Hrouda, F. Magnetic anisotropy of rocks and its application in geology and geophysics. *Geophys. Surv.* **1982**, *5*, 37–82. [CrossRef]
22. Tarling, D.H.; Hrouda, F. *The Magnetic Anisotropy of Rocks*; Magnetite-Series and Ilmenite-Series; Chapman & Hall: London, UK, 1993; 217p.
23. Siegesmund, S.; Ullemeyer, K.; Dahms, M. Control of magnetic rock fabrics by mica preferred orientation: A quantitative approach. *J. Struct. Geol.* **1995**, *17*, 1601–1613. [CrossRef]
24. Lowrie, W. *Fundamentals of Geophysics*; Cambridge University Press: Cambridge, UK, 2007.
25. Nédéléc, A.; Bouchez, J.L. *Granites: Petrology, Structure, Geological Setting, and Metallogeny*; Oxford University Press: London, UK, 2015; p. 335.
26. Hrouda, F. Magnetic Susceptibility, Anisotropy. In *Encyclopedia of Geomagnetism and Paleomagnetism*; Gubbins, D., Herrero-Bervera, E., Eds.; Springer: Berlin/Heidelberg, Germany, 2007; pp. 546–558.
27. Matte, P.; Ribeiro, A. Forme et orientation de l'ellipsoïde de déformation dans la virgation hercynienne de Galice. Relations avec le plissement et hypothèses sur la genèse de l'arc Ibéro-Armoricain. *C R Hebd Séanc Acad. Sci. Sér. D* **1975**, *280*, 2825–2828.
28. Matte, P. La chaine varisque parmi les chaines periatlantiques: Modele d'evolution et position des grandes blocs continentaux au Permo-Carbonifere. *Bill. Soc. Geol. France* **1986**, *2*, 1–24.
29. Crespo-Blanc, A. Evolución Geotectónica del Contacto Entre la Zona de Ossa-Morena y la Zona Surportuguesa em las Sierras de Aracena y Aroche (Macizo Ibérico Meridional): Um Contacto Mayor em la Cadena Hercínica Europea. Ph.D. Thesis, University of Sevilha, Sevilha, Spain, 1989.
30. Ribeiro, A.; Munhá, J.; Dias, R.; Mateus, A.; Pereira, E.; Ribeiro, M.L.; Fonseca, P.; Araújo, A.; Oliveira, T.; Romão, J.; et al. Geodynamic evolution of SW Europe Variscides. *Tectonics* **2007**, *26*, 1–24. [CrossRef]
31. Lotze, F. Zur gliederung der Varisziden der Iberischen Meseta. *Geoteckt. Forsch.* **1945**, *6*, 78–92.
32. Farias, P.; Gallastegui, G.; Gonzalez Lodeiro, F.; Marquinez, J.; Martin Parra, L.M.; Martínez Catalan, J.R.; de Pablo Maciá, J.G.; Rodriguez Fernandez, L.R. Aportaciones al conocimiento de la litoestratigrafia y estructura de Galícia Central. In Proceedings of the IX Reunião de Geologia do Oeste Peninsular, Porto, Portugal, 4 October 1985; Memórias do Museu e Laboratório Mineralógico e Geológico da Faculdade Ciências Universidade Porto: Porto, Portugal, 1987; Volume 1, pp. 411–431.
33. Ribeiro, A.; Pereira, E.; Dias, R. Structure in the northwest of the Iberian Peninsula. In *Pre-Mesozoic Geology of Iberia*; Dallmeyer, R.D., Martínez Garcia, E., Eds.; Springer: Berlin/Heidelberg, Germany, 1990; pp. 220–236.
34. Quesada, C. Geological constraints on the Paleozoic tectonic evolution of tectonostratigraphic terranes in the Iberian Massif. *Tectonophysics* **1991**, *185*, 225–245. [CrossRef]
35. Matte, P. The Variscan collage and orogeny (480–290 Ma) and the tectonic definition of the Armorica microplate: A review. *Terra Nova* **2001**, *13*, 122–128. [CrossRef]
36. Pérez-Estaún, A.; Bastida, F.; Alonso, J.L.; Marquínez, J.; Aller, J.; Alvarez-Marrón, J.; Marcos, A.; Pulgar, J.A. A thin-skinned tectonics model for an arcuate fold and thrust belt: The Cantabrian Zone (Variscan Ibero-Armorican Arc). *Tectonics* **1988**, *7*, 517–537. [CrossRef]
37. Aerden, D.G.A.M. Correlating deformation in Variscan NW-Iberia using porphyroblasts; implications for the Ibero-Armorican Arc. *J. Struct. Geol.* **2004**, *26*, 177–196. [CrossRef]

38. Martínez Catalán, J.R. Are the oroclines of the Variscan belt related to late Variscan strike-slip tectonics? *Terra Nova* **2011**, *23*, 241–247. [CrossRef]
39. Martínez Catalán, J.R. The Central Iberian arc, an orocline cen- tered in the Iberian Massif and some implications for the Variscan belt. *Int. J. Earth Sci.* **2012**, *101*, 1299–1314. [CrossRef]
40. Martinéz Cátalan, J.R.; Arenas, R.; Abati, J.; Sánchez Martínez, S.; Díaz García, F.; Fernández Suárez, J.; González Cuadra, P.; Castiñeiras, P.; Gómez Barreiro, J.; Díez Montes, A.; et al. A rootless suture and the loss of the roots of a mountain chain: The Variscan belt of NW Iberia. *Comptes Rendus Geosci.* **2009**, *341*, 114–126. [CrossRef]
41. Gutiérrez-Alonso, G.; Fernández-Suárez, J.; Jeffries, T.E.; Johnston, S.T.; Pastor-Galán, D.; Murphy, J.B.; Franco, M.P.; Gonzalo, J.C. Diachronous post-orogenic magmatism within a developing orocline in Iberia European Variscides. *Tectonics* **2011**, *30*, TC5008. [CrossRef]
42. Pastor-Galán, D.; Gutiérrez-Alonso, G.; Weil, A.B. Orocline tim- ing through joint analysis: Insights from the Ibero-Armorican Arc. *Tectonophysics* **2011**, *507*, 31–46. [CrossRef]
43. Pastor-Galán, D.; Groenewegen, T.; Brouwer, D.; Krijgsman, W.; Dekkers, M.J. One or two oroclines in the Variscan orogen of Iberia? Implications for Pangea Amalgamation. *Geology* **2015**, *43*, 527–530. [CrossRef]
44. Pastor-Galán, D.; Ursem, B.; Meere, P.A.; Langereis, C. Extending the Cantabrian Orocline to two continents (from Gondwana to Laurussia). Paleomagnetism from South Ireland. *Earth Planet. Sci. Lett.* **2015**, *432*, 223–231. [CrossRef]
45. Shaw, J.; Johnston, S.T.; Gutiérrez-Alonso, G.; Weil, A.B. Oroclines of the Variscan orogen of Iberia: Paleocurrent analysis and paleogeographic implications. *Earth Planet. Sci. Lett.* **2012**, *329–330*, 60–70. [CrossRef]
46. Ribeiro, A. Contribution à L'étude de Trás-os-Montes Oriental. Serviços Geológicos de Portugal. Ph.D. Thesis, Memórias dos Serviços Geológicos Portugal, Lisboa, Portugal, 1974.
47. Noronha, F.; Ramos, J.M.F.; Rebelo, J.A.; Ribeiro, A.; Ribeiro, M.L. Essai de corrélation des phases de déformation hercynienne dans le Nord-Ouest Péninsulaire. *Bol. Soc. Geol. Port.* **1979**, *21*, 227–237.
48. Pereira, M.F.; Gama, C.; Rodríguez, C. Coeval interaction between magmas of contrasting composition (Late Carboniferous–Early Permian Santa Eulália–Monforte massif, Ossa-Morena Zone): Field relationships and geochronological constraints. *Geol. Acta* **2017**, *15*, 409–428. [CrossRef]
49. Hildenbrand, A.; Marques, F.O.; Quidelleur, X.; Noronha, F. Exhumation history of the Variscan orogen in western Iberia as inferred from new K-Ar and $^{40}Ar/^{39}Ar$ data on granites from Portugal. *Tectonophysics* **2021**, *812*, 228863. [CrossRef]
50. Martínez Catalán, J.R.; Rubio Pascual, F.J.; Díez Montes, A.; Díez Fernández, R.; Gómez Barreiro, J.; Dias da Silva, Í.; González Clavijo, E.; Ayarza, P.; Alcock, J.E. The late Variscan HT/LP metamorphic event in NW and Central Iberia: Relationships to crustal thickening, extension, orocline development and crustal evolution. *Geol. Soc. Lond. Spec. Publ.* **2014**, *405*, 225–247. [CrossRef]
51. Ferreira, N.; Iglésias, M.; Noronha, F.; Pereira, E.; Ribeiro, A.; Ribeiro, M.L. Granitóides da Zona Centro Ibérica e seu enquadramento geodinâmico. In *Geología de los Granitoides y Rocas Asociadas del Macizo Hesperico Libro de Homenaje a L.C. García de Figuerola*; Bea, F., Carnicero, A., Gonzalo, J., Plaza, M.L., Alonso, M.R., Eds.; Editorial Rueda: Madrid, Spain, 1987; pp. 37–51.
52. Dias, G.; Leterrier, J.; Mendes, A.; Simões, P.; Bertrand, J.M. U-Pb zircon and monazite geochronology of syn- to post-tectonic Hercynian granitoids from the Central Iberian Zone (Northern Portugal). *Lithos* **1998**, *45*, 349–369. [CrossRef]
53. Dias, G.; Noronha, F.; Ferreira, N. *Variscan Plutonism in the Central Iberian Zone (Northern Portugal)*; Eurogranites, Field Meeting, Guidebook; Universidade do Minho: Guimarães, Portugal, 2000.
54. Martins, H.C.B. Geoquímica e Petrogénese de Granitóides Tarditectónicos e Pós-Tectónicos. Implicações Metalogénicas. Ph.D. Thesis, University of Trás-os-Montes e Alto Douro, Vila Real, Portugal, 1998.
55. Neiva, A.M.R. Portuguese Granites Associated with Sn-W and Au Mineralizations. *Bull. Geol. Soc. Finl.* **2002**, *74*, 79–101. [CrossRef]
56. Pereira, M.F.; Díez Fernández, R.; Gama, C.; Hofmann, M.; Gärtner, A.; Linnemann, U. S-type granite generation and emplacement during a regional switch from extensional to contractional deformation (Central Iberian Zone, Iberian autochthonous domain, Variscan Orogeny). *Int. J. Earth Sci.* **2018**, *107*, 251–267. [CrossRef]
57. Capdevila, R.; Corretgé, L.G.; Floor, P. Les granitoïdes Varisques de la Méséta Ibérique. *Bull. Société Géologique Fr.* **1973**, *80*, 209–228. [CrossRef]
58. Bea, F.; Montero, P.; Molina, J.F. Mafic Precursors, Peraluminous Granitoids, and Late Lamprophyres in the Avila Batholith: A Model for the Generation of Variscan Batholiths in Iberia. *J. Geol.* **1999**, *107*, 399–419. [CrossRef]
59. Dias, R.; Ribeiro, A.; Romão, J.; Coke, C.; Moreira, N. A review of the arcuate structures in the Iberian Variscides; constraints and genetic models. *Tectonophysics* **2016**, *681*, 170–194. [CrossRef]
60. Chappell, B.W.; White, A.J.R. Two contrasting granite types. *Pac. Geol.* **1974**, *8*, 173–174.
61. Orejana, D.; Villaseca, C.; Pérez-Soba, C.; López-Garcia, J.; Billstrom, K. The Variscan gabbros from the Spanish Central System: A case for crustal recycling in the sub-continental lithospheric mantle? *Lithos* **2009**, *110*, 262–276. [CrossRef]
62. Villaseca, C.; Belousova, E.; Orejana, D.; Castiñeiras, P.; Pérez-Soba, C. Presence of Palaeoproterozoic and Archean components in the granulite-facies rocks of central Iberia: The Hf isotopic evidence. *Precambrian Res.* **2011**, *187*, 143–154. [CrossRef]
63. Gonçalves, A.; Sant'Ovaia, H.; Noronha, F. Petrofabric patterns of two contrasting plutons: Example of Penedos and Borralha granites (Montalegre, Northern Portugal). In Proceedings of the EGU General Assembly Conference Abstracts, Vienna, Austria, 23–27 May 2022.

64. Gonçalves, A.; Sant'Ovaia, H.; Noronha, F. Zircon U-Pb dating and Lu-Hf isotopes of granite intrusions from North and Central Portugal: Emplacement age and source of magma. In Proceedings of the Congresso Nacional de Geologia, Coimbra, Portugal, 17–19 July 2023.
65. Almeida, A.; Leterrier, J.; Noronha, F.; Bertrand, J.M. U-Pb zircon and monazite geochronology of the Hercynian two mica granite composite pluton of Cabeceiras de Basto (Northern Portugal). *Comptes Rendus L'académie Sci.* **1998**, *326*, 779–785.
66. Almeida, A.; Santos, J.F.; Noronha, F. Contribuição dos sistemas isotópicos Sm-Nd e Rb-Sr para o estudo petrogenético do maciço granítico peraluminoso de duas micas da cidade do Porto (NW Portugal). *Com. Geol. Port.* **2014**, *101*, 27–30.
67. Antunes, I.M.H.R.; Neiva, A.M.R.; Silva, M.M.V.G. Isotopic geochronology of granitic rocks from the Central Iberian Zone: Comparison of methodologies. *Estud. Geológicos* **2010**, *66*, 45–50. [CrossRef]
68. Martins, H.C.B.; Sant'Ovaia, H.; Noronha, F. Late-Variscan emplacement and genesis of the Vieira do Minho composite pluton, Central Iberian Zone: Constraints from U–Pb zircon geochronology, AMS data and Sr–Nd–O isotope geochemistry. *Lithos* **2013**, *162–163*, 221–235. [CrossRef]
69. Gonçalves, A. Role of the Late-Variscan Structures in the Emplacement of Late-Orogenic Granitoids in NW Iberian Peninsula. Metallogenic Implications in the Occurrence of W(Sn) Mineralizations; Faculdade de Ciências da Universidade do Porto, Universidade de Aveiro, Aveiro, Portugal, 2021; 396p. Available online: https://hdl.handle.net/10216/138508 (accessed on 10 December 2023).
70. Gonçalves, A.; Sant'Ovaia, H.; Martins, H.C.B.; Noronha, F. Magnetic fabrics and emplacement mechanisms of Valpaços and Freixo de Numão Variscan Granites (Northern Portugal). *Int. J. Earth Sci.* **2022**, *111*, 1437–1468. [CrossRef]
71. Neiva, A.M.R.; Williams, I.S.; Ramos, J.M.F.; Gomes, M.E.P.; Silva, M.M.V.G.; Antunes, I.M.H.R. Geochemical and isotopic constraints on the petrogenesis of Early Ordovician granodiorite and Variscan two-mica granites from the Gouveia area, central Portugal. *Lithos* **2009**, *111*, 186–202. [CrossRef]
72. Sant'ovaia, H.; Olivier, P.; Ferreira, N.; Noronha, F.; Leblanc, D. Magmatic structures and kinematics em-placement of the Variscan granites from Central Portugal (Serra da Estrela and Castro Daire areas). *J. Struct. Geol.* **2010**, *32*, 1450–1465. [CrossRef]
73. Costa, M. Geoquímica dos Granitóides de Aguiar da Beira, Norte de Portugal. Ph.D. Thesis, Universidade de Aveiro, Aveiro, Portugal, 2011.
74. Corrêa-Ribeiro, H. Génese e Cinemática de Instalação do Plutão Granítico de Valpaços. Ph.D. Thesis, Universidade do Porto, Porto, Portugal, 2018.
75. Gonçalves, A.; Sant'ovaia, H.; Noronha, F. Geochemical Signature and Magnetic Fabric of Capinha Massif (Fundão, Central Portugal): Genesis, Emplacement and Relation with W–Sn Mineralizations. *Minerals* **2020**, *10*, 557. [CrossRef]
76. Mota Leite, S.; Santos, J.; Azevedo, M. Variscan plutonism in the Castro Daire area (Northern Central Portugal) e constraints from U-Pb geochronology. In Proceedings of the 6th International Symposium on Applied Isotope Geochemistry, Prague, Czech Republic, 11–16 September 2005.
77. Fernandes, S.; Gomes, M.; Teixeira, R.; Corfu, F. Geochemistry of biotite granites from the Lamas de Olo Pluton, northern Portugal. *Geophys. Res. Abstr.* **2013**, *15*, EGU2013-11566.
78. Cruz, C. Post-Tectonic Variscan Magmatism from Northwest Iberia. Implications for W-Mo Metallogeny. Case Study of Lamas de Olo Pluton. Ph.D. Thesis, Faculdade de Ciências da Universidade do Porto, Universidade de Aveiro, Aveiro, Portugal, 2020; 252p. Available online: https://hdl.handle.net/10216/129301 (accessed on 10 December 2023).
79. Sant'Ovaia, H.; Bouchez, J.L.; Noronha, F.; Leblanc, D.; Vigneresse, J.L. Composite-laccolith emplacement of the post-tectonic Vila Pouca de Aguiar granite pluton (northern Portugal): A combined AMS and gravity study. *Earth Environ. Sci. Trans. R. Soc. Edinb.* **2000**, *91*, 123–137.
80. Martins, H.C.B.; Sant'Ovaia, H.; Abreu, J.; Oliveira, J.; Noronha, F. Emplacement of the Lavadores granite (NW Portugal): U/Pb and AMS results. *Comptes Rendus Geosci.* **2011**, *343*, 387–396. [CrossRef]
81. Sant'Ovaia, H.; Ribeiro, M.A.; Martins, H.; Ferrão, F.; Gomes, C.; Noronha, F. Estruturas e fabric magnético no maciço granítico de Lavadores-Madalena. *Comun. Geológicas* **2014**, *101*, 313–318.
82. Gonçalves, A.; Sant'Ovaia, H.; Ribeiro, M.A.; Noronha, F. The Esmolfe-Matança granite (Penalva do Castelo, Central Portugal): A keystone to understand the ascent and emplacement of magmas under low tectonic stress. *J. Struct. Geol.* **2020**, *139*, 104–143. [CrossRef]
83. Simões, P.P.; Sant'Ovaia, H.; Martins, H.C.B.; Dias, G. The Fe-K subalkaline Monçao-Porriño pluton (NW Portugal): Genesis, fabric and SHRIMP U-Pb zircon geochronology. In Proceedings of the IX Congreso Ibérico—XI Congreso Nacional de Geoquímica, Soria, Spain, 16–17 September 2013; pp. 22–23.
84. Bouchez, J.L. Magnetic susceptibility anisotropy and fabrics in granites. *Comptes Rendus L'académie Sci. Terre Planètes—Earth Planet. Sci.* **2000**, *330*, 1–14.
85. Rochette, P.; Jackson, M.; Aubourg, C. Rock magnetism and the interpretation of magnetic susceptibility. *Rev. Geophys.* **1992**, *30*, 209–226. [CrossRef]
86. Ishihara, S. The magnetite-series and ilmenite-series granitic rocks. *Min. Geol.* **1977**, *27*, 293–305. [CrossRef]
87. Ildefonse, B.; Fernandez, A. Influence of the concentration of rigid markers in a viscous medium on the production of preferred orientations. An experimental contribution, 1. Non-coaxial strain. *Bull. Geol. Inst. Univ. Upps.* **1988**, *14*, 55–60.
88. Paterson, S.R.; Vernon, R.H.; Tobisch, O.T. A review criteria for the identification of magmatic and tectonic foliations in granitoids. *J. Struct. Geol.* **1989**, *11*, 349–363. [CrossRef]

89. Burton-Johnson, A.; Macpherson, C.G.; Muraszko, J.R.; Harrison, R.J.; Jordan, T.A. Tectonic strain recorded by magnetic fabrics (AMS) in plutons, including Mt Kinabalu, Borneo: A tool to explore past tectonic regimes and syn-magmatic deformation. *J. Struct. Geol.* **2019**, *119*, 50–60. [CrossRef]
90. Burton-Johnson, A.; Riley, T.R.; Harrison, R.J.; Mac Niocaill, C.; Muraszko, J.R.; Rowley, P.D. Does tectonic deformation control episodic continental arc magmatism? Evidence from granitic magnetic fabrics (AMS). *Gondwana Res.* **2022**, *112*, 1–23. [CrossRef]
91. Horsman, E.; Tikoff, B.; Morgan, S. Emplacement-related fabric and multiple sheets in the Maiden Creek sill, Henry Mountains, Utah, USA. *J. Struct. Geol.* **2005**, *27*, 1426–1444. [CrossRef]
92. Stevenson, C.T.E.; Owens, W.H.; Hutton, D.H.W.; Hood, D.N.; Meighan, I.G. Laccolithic, as opposed to cauldron subsidence, emplacement of the Eastern Mourne pluton, N. Ireland: Evidence from anisotropy of magnetic susceptibility. *J. Geol. Soc.* **2007**, *164*, 99–110. [CrossRef]
93. Clemens, J.D.; Mawer, C.K. Granitic magma transport by fracture propagation. *Tectonophysics* **1992**, *204*, 339–360. [CrossRef]
94. Vigneresse, J.L.; Tikoff, B.; Améglio, L. Modification of the regional stress field by magma intrusion and formation of tabular granitic plutons. *Tectonophysics* **1999**, *302*, 203–224. [CrossRef]
95. Benn, K.; Home, R.J.; Kontak, D.J.; Pignotta, G.; Evans, N.G. Syn-Acadian emplacement model for the South Mountain Batholith, Meguma Terrane, Nova Scotia: Magnetic fabric and structural analyses. *Geol. Soc. Am. Bull.* **1997**, *109*, 1279–1293. [CrossRef]
96. Benn, K. Anisotropy of magnetic susceptibility fabrics in syntectonic plutonsas tectonic strain markers: Example of the Canso pluton, Meguma Terrane, Nova Scotia. *Earth Environ. Sci. Trans. R. Soc. Edinb.* **2010**, *100*, 147–158. [CrossRef]
97. Petronis, M.S.; O'Driscoll, B.; Stevenson, C.T.E.; Reavy, R.J. Controls on emplacement of the Caledonian Ross of Mull Granite, NW Scotland: Anisotropy of magnetic susceptibility and magmatic and regional structures. *GSA Bull.* **2012**, *124*, 906–927. [CrossRef]
98. Olivier, P.; de Saint Blanquant, M.; Gleizes, G.; Leblanc, D. Homogeneity of granitic fabrics at the metre and dekametre scales. In *Granite: From Segregation of Melt to Emplacement Fabrics*; Bouchez, J.L., Hutton, D.H.W., Stephens, W.E., Eds.; Kluwer Academic Publishers: Dordrecht, The Nederland, 1997; pp. 113–127.
99. Cruz, C.; Sant'Ovaia, H.; Noronha, F. Magnetic susceptibility and δ18O characterization of Variscan granites related to W–(Mo) and Sn–(W) mineralizations: Lamas de Olo Pluton case study. *Comun. Geológicas* **2016**, *103*, 143–174.
100. Gonçalves, A.; Sant'Ovaia, H.; Noronha, F. Role of Variscan granites in the genesis of Freixo de Numão W(Sn) district (Northern Portugal). *J. Iber. Geol.* **2022**, *48*, 309–353. [CrossRef]
101. Sant'Ovaia, H.; Noronha, F. Gravimetric anomaly modelling of the post-tectonic granite pluton of Águas Frias—Chaves (Northern Portugal). *Cuad. Lab. Xeolóxico Laxe* **2005**, *30*, 87–98.
102. Frost, B.R.; Lindsley, D.H.; Andersen, D.J. Fe-Ti oxide-silicate equilibria: Assemblages with fayalitic olivine. *Am. Mineral.* **1988**, *73*, 727–740.
103. Fuhrman, M.L.; Frost, B.R.; Lindsey, D.H. The petrology of the Sybille Monzosyenite, Laramie Anorthosite Complex, Wyoming. *J. Petrol.* **1988**, *29*, 669–729. [CrossRef]
104. Villaseca, C.; Ruiz-Martínez, V.C.; Pérez-Soba, C. Magnetic susceptibility of Variscan granite-types of the Spanish Central System and the redox state of magma. *Geol. Acta* **2017**, *15*, 379–394.